

AD-A274 874



WL-TR-93-2097



**THE IMPORTANCE OF VIBRATIONALLY
EXCITED NITROGEN IN SILICON NITRIDE
DEPOSITION SYSTEMS**

DTIC
ELECTE
JAN 25 1994
S c D

LAWRENCE G. PIPER

**PHYSICAL SCIENCES, INC
20 NEW ENGLAND BUSINESS CENTER
ANDOVER, MA 01810**

AUGUST 1993

FINAL REPORT FOR PERIOD 05/01/91 - 05/01/93

APPROVED FOR PUBLIC RELEASE; DISTRIBUTION UNLIMITED.

**AERO PROPULSION AND POWER DIRECTORATE
WRIGHT LABORATORY
AIR FORCE SYSTEMS COMMAND
WRIGHT-PATTERSON AIR FORCE BASE, OH 45433-7650**

94 1 24 004

52A **94-02046**





NOTICE


When Government drawings, specifications, or other data are used for any purpose other than in connection with a definitely Government-related procurement, the United States Government incurs no responsibility or any obligation whatsoever. The fact that the government may have formulated or in any way supplied the said drawings, specifications, or other data, is not to be regarded by implication, or otherwise in any manner construed, as licensing the holder, or any other person or corporation; or as conveying any rights or permission to manufacture, use, or sell any patented invention that may in any way be related thereto.

This report is releasable to the National Technical Information Service (NTIS). At NTIS, it will be available to the general public, including foreign nations.

This technical report has been reviewed and is approved for publication.


CHARLES A. DEJOSEPH JR
Advanced Plasma Research Section
Power Components Branch
Aerospace Power Division
Aero Propulsion and Power Directorate


JERRELL M. TURNER
Chief, Advanced Plasma Research Section
Power Components Branch
Aerospace Power Division
Aero Propulsion and Power Directorate


MICHAEL D. BRAYDICH, Lt Col, USAF
Deputy Chief
Aerospace Power Division
Aero Propulsion & Power Directorate

If your address has changed, if you wish to be removed from our mailing list, or if the addressee is no longer employed by your organization please notify WL/POOC, WPAFB, OH 45433-7919 to help us maintain a current mailing list.

Copies of this report should not be returned unless return is required by security considerations, contractual obligations, or notice on a specific document.

REPORT DOCUMENTATION PAGE			Form Approved OMB No. 0704-0188	
<small>Public reporting burden for this collection of information is estimated to average 1 hour per response, including the time for reviewing instructions, searching existing data sources, gathering and maintaining the data needed, and completing and reviewing the collection of information. Send comments regarding this burden estimate or any other aspect of this collection of information, including suggestions for reducing this burden, to Washington Headquarters Services, Directorate for Information Operations and Reports, 1215 Jefferson Davis Highway, Suite 1204, Arlington, VA 22202-4302, and to the Office of Management and Budget, Paperwork Reduction Project (0704-0188), Washington, DC 20503.</small>				
1. AGENCY USE ONLY (Leave blank)	2. REPORT DATE October 1993	3. REPORT TYPE AND DATES COVERED Final 3 May 1991 - 2 May 1993		
4. TITLE AND SUBTITLE The Importance of Vibrationally Excited Nitrogen in Silicon Nitride Deposition Systems		5. FUNDING NUMBERS C F33615-91-C-2112 PE 61102F PR 2301 TA S2 WU 02		
6. AUTHOR(S) Lawrence G. Piper				
7. PERFORMING ORGANIZATION NAME(S) AND ADDRESS(ES) Physical Sciences Inc. 20 New England Business Center Andover, MA 01810-1077		8. PERFORMING ORGANIZATION REPORT NUMBER PSI-1126/TR-1257		
9. SPONSORING/MONITORING AGENCY NAME(S) AND ADDRESS(ES) Aero Propulsion and Power Directorate Wright Laboratory Wright-Patterson AFB, OH 45433-6563		10. SPONSORING/MONITORING AGENCY REPORT NUMBER WL-TR-93-2097		
11. SUPPLEMENTARY NOTES				
12a. DISTRIBUTION/AVAILABILITY STATEMENT APPROVED FOR PUBLIC RELEASE; DISTRIBUTION UNLIMITED			12b. DISTRIBUTION CODE	
13. ABSTRACT (Maximum 200 words) <p>We have studied the kinetics of $N_2(X,v)$ with silane in a discharge-flow reactor using metastable energy transfer diagnostics. $N_2(B^3\Pi_g, v' \leq 12)$ fluorescence, excited in the interaction between metastable $N_2(A^3\Sigma_u^+)$ and $N_2(X^1\Sigma_g^+, v)$, monitored vibrational levels between five and at least thirteen, while $N_2^+(B^2\Sigma_g^+, v'=0-8)$ fluorescence, excited by metastable helium atoms, diagnoses vibrational levels between one and six. The rate coefficients for quenching vibrationally excited nitrogen by silane range from 1 to $6 \times 10^{-13} \text{ cm}^3 \text{ molecule}^{-1} \text{ s}^{-1}$, being higher for the higher vibrational levels.</p> <p>Observations at 4500 nm show that about 15% of the $N_2(X,v)$ quenching events excite $\text{SiH}_4(\nu_3)$. Presumably the rest of the energy is absorbed by other vibrational modes.</p>				
14. SUBJECT TERMS KINETICS OF $N_2(x,v)$ VIBRATIONAL MODES		METASTABLE ENERGY TRANSFER DIAGNOSTICS DISCHARGE-FLOW REACTOR		15. NUMBER OF PAGES 46
				16. PRICE CODE
17. SECURITY CLASSIFICATION OF REPORT Unclassified	18. SECURITY CLASSIFICATION OF THIS PAGE Unclassified	19. SECURITY CLASSIFICATION OF ABSTRACT Unclassified	20. LIMITATION OF ABSTRACT Unlimited	

CLASSIFIED BY

DECLASSIFY ON

In a separate series of experiments silane was added to an active nitrogen discharge afterglow and the reaction products impinged upon a heated single crystal silicon substrate further downstream. Infrared absorption spectroscopy showed that the coatings generated were silicon nitride, although some hydrogen was incorporated into the films. In addition, the active nitrogen/silane interaction generated a quantity of fine (micron sized particles), white silicon nitride powder.

TABLE OF CONTENTS

1.	SUMMARY	1
2.	INTRODUCTION	3
3.	EXPERIMENTAL	7
4.	ENERGY-TRANSFER BASED DIAGNOSTICS OF $N_2(X, v)$	11
4.1	Penning Ionization	12
4.2	$N_2(A)$ Energy Transfer	13
5.	$N_2(X, v)$ QUENCHING BY SiH_4	15
5.1	Experimental Approach	15
5.2	Results for $N_2(X, v \geq 5)$	17
5.3	Results for $N_2(X, v \leq 6)$	20
6.	$SiH_4(\nu_3)$ EXCITATION BY $N_2(X, v)$	28
7.	ALTERNATIVE DETERMINATION OF $N_2(X, v)$ QUENCHING RATE COEFFICIENTS	35
8.	SILICON NITRIDE COATING EXPERIMENTS	38
9.	CONCLUSIONS AND SUGGESTIONS FOR FURTHER STUDY	41
10.	REFERENCES	42

DTIC QUALITY INSPECTED 8

Accession For	
NTIS CRA&I	<input checked="checked" type="checkbox"/>
DTIC TAB	<input type="checkbox"/>
Unannounced	<input type="checkbox"/>
Justification	
By	
Distribution /	
Availability Codes	
Dist	Avail and/or Special
A-1	

LIST OF FIGURES

1	Discharge flow reactor for studying the kinetics of reactions involving $N_2(X, v)$	7
2	Schematic of apparatus for observing $SiH_4(\nu_3)$ infrared emission	9
3	Schematic of apparatus for coating substrates with silicon nitride	10
4	Variation in the $N_2(B-A)$ intensity excited in the $N_2(A) + N_2(X, v)$ reaction, as a function of reaction time and SiH_4 number density	16
5	Net quenching of $N_2(X, v \geq 6)$ by silane	18
6	Net quenching of $N_2(X, v \geq 9)$ by SiH_4	19
7	Net quenching by $N_2(X, v \geq 11)$ by SiH_4	20
8	Net quenching of $N_2(X, v=2)$ by SiH_4	22
9	Net quenching of $N_2(X, v=4)$ by SiH_4	23
10	Single quantum analysis of quenching of $N_2(X, v=1)$ by SiH_4	25
11	Single quantum transfer analysis of the quenching of $N_2(X, v=3)$ by SiH_4	26
12	Analysis of the quenching of $N_2(X, v=1)$ by SiH_4 from observations of the increase in $[N_2(X, v=0)]$ as a function of $[SiH_4]$	27
13	Spectrum of $SiH_4(\nu_3)$ emission excited by $N_2(v)$	28
14	Spectrum of $N_2O(\nu_3)$ emission excited by $N_2(v)$	29
15	Intensity of $SiH_4(\nu_3)$ as a function of $[SiH_4]$ added to $N_2(X, v)$	29
16	Intensity of $SiH_4(\nu_3)$ emission as a function of $[SiH_4]$ added to $N_2(X, v)$	32
17	Excitation of $SiH_4(\nu_3)$ by $N_2(X, v)$ at various total argon pressures compared to a kinetic model	33
18	Excitation of $N_2O(\nu_3)$ by $N_2(X, v)$ at various total pressures of argon compared to a kinetic model	34

LIST OF FIGURES (Continued)

19	Quenching of $N_2(X, v)$ by SiH_4 using $N_2O(\nu_3)$ fluorescence as a monitor of $[N_2(X, v)]$	36
20	Infrared absorption spectrum of Si_3N_4 on single-crystal silicon	38
21	Infrared absorption spectrum of silicon nitride powder in a KBr pellet	39

LIST OF TABLES

1	Rate Coefficients for $N_2(X,v)$ and $N_2(B^3\Pi_g)$ Quenching by SiH_4	21
2	Rate Coefficients for Relaxation of $N_2(X,v)$ Using Penning-ionization Diagnostic	24

1. SUMMARY

We have investigated the kinetics of $N_2(X, v)$ quenching by silane. These studies were a first step in understanding the kinetic processes important in silicon nitride coating systems using the remote plasma enhanced chemical vapor deposition technique. Our experiments were carried out in a discharge-flow reactor and used metastable energy transfer diagnostics to detect $N_2(X, v)$ in vibrational levels from zero up to at least 13.

We used metastable helium Penning ionization to detect vibrational levels between zero and six, and $N_2(A)$ energy transfer to detect levels from five up to at least 13. Metastable helium excites $N_2(X, v)$ to $N_2^+(B^2\Sigma^+)$. By analyzing the resultant $N_2^+(B^2\Sigma^+-X)$ fluorescence we can determine the vibrational populations of $N_2(X, v)$ quantitatively. $N_2(A^3\Sigma_u^+)$ excites $N_2(X, v)$ to $N_2(B^3\Pi_g)$. Analysis of the subsequent $N_2(B^3\Pi_g-A^3\Sigma_u^+)$ fluorescence gives a semiquantitative estimate of the vibrational distributions for levels from 5 up to at least 13.

We measured the rate coefficients by monitoring the decrease in the populations of $N_2(X, v)$ as a function of $[SiH_4]$ and time between the injection of the silane and detection of the $N_2(X, v)$. We analyzed our data assuming an exponential decay of the $N_2(X, v)$ level under investigation. In addition, the data for vibrational levels 0 through 6 were analyzed according to a single-quantum transfer model. The exponential decay analysis only gives the effective removal of $N_2(X, v)$ in the observed vibrational level, essentially the difference between the removal of vibrational energy from a given level to those below it and the feed into the vibrational level from those above it. The single-quantum transfer model, on the other hand accounts for feed from higher vibrational levels. Our results indicate that the rate coefficient for quenching $N_2(X, v)$ by silane varies from about $1 \times 10^{-13} \text{ cm}^3 \text{ molecule}^{-1} \text{ s}^{-1}$ for $v=1$ up to about $6 \times 10^{-13} \text{ cm}^3 \text{ molecule}^{-1} \text{ s}^{-1}$ for vibrational levels above 5.

We detected fluorescence from $SiH_4(\nu_3)$ at 4500 nm when silane and $N_2(X, v)$ were mixed, thus indicating that one channel for the quenching reaction is vibration-vibration (v-v) energy transfer. Comparing the relative excitation rate coefficients of $SiH_4(\nu_3)$ and $N_2O(\nu_3)$, excited when N_2O was added to a flow of $N_2(X, v)$, indicated that only about 15% of the total $N_2(X, v)$ quenching results in $SiH_4(\nu_3)$ excitation. This assumes that $N_2O(\nu_3)$ excitation is the only channel for $N_2(X, v)$ quenching by N_2O . Presumably the rest of the quenching appears in other vibrational modes of SiH_4 , although ν_3 excitation would be expected to be favored since v-v transfer to ν_3 is resonant to within kT for single quantum transfer from all $N_2(X, v)$ vibrational levels below 16.

We had planned to investigate the possibility that $N_2(X, v)$ quenching would lead to SiH_4 dissociation by monitoring H-atom production using vacuum ultraviolet (vuv) resonance fluorescence at 121.6 nm. Unfortunately, our vuv detection sensitivity below 130 nm was so small H-atom resonance fluorescence was undetectable even when significant number densities of H atoms were purposely added to the reactor. This degeneration seems to be a recent problem since our system sensitivity was quite good several years ago.

We began a series of experiments in which we coated single crystal silicon chips with silicon nitride. These experiments were performed in another discharge-flow reactor. In this apparatus, active nitrogen was generated in a microwave discharge sustained in a flowing mixture of nitrogen in argon. Silane was added to the discharge afterglow and the reaction products impinged upon a heated substrate further downstream. Infrared absorption spectroscopy showed that the coatings generated were indeed silicon nitride, although some hydrogen was incorporated into the films. In addition to the coatings, the active nitrogen/silane interaction generated a quantity of fine (micron sized particles), white powder. Infrared absorption spectroscopy indicated this powder to be silicon nitride.

2. INTRODUCTION

Silicon nitride films find wide application as abrasion-, corrosion-, and oxidation-resistant coatings to protect machined parts in high temperature environments. They are used in numerous ways including radiant heat shields, rocket nozzle inserts and crucibles for melting and refining. Some applications require relatively cool substrate temperatures during the coating process so that other species on the substrate don't evaporate or migrate to undesirable areas of the substrate. The limited mechanical strength of some substrate structures necessitates cool substrate temperatures during the coating process.¹

Switching from normal chemical vapor deposition (CVD), for which substrate temperatures typically are 700 to 1000°C, to plasma enhanced chemical vapor deposition (PECVD) allows coating down to temperatures on the order of 200 to 500°C.² Typical conditions for PECVD involve placing the substrate to be coated inside a discharge maintained in mixture of SiH₄ and either N₂ or NH₃. This procedure typically results in the incorporation of between 10 and 30 atom percent hydrogen in the coating. For some applications, this level of hydrogen is unacceptable.

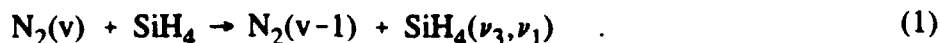
A variation of PECVD, which also is suitable for substrate temperatures on the order of 200 to 500°C, and which results in undetectable concentrations of Si-H or N-H bonds in deposited films, has been dubbed by one of its developers "remote plasma enhanced chemical vapor deposition" (RPECVD).³ In this technique, the discharge is removed from the substrate. Silane is added to the effluents of a discharge in flowing nitrogen. Energetic species in the discharged nitrogen (generally called "active nitrogen") decompose the silane; the reaction products from this decomposition then impinge upon the substrate and lay down a film of silicon nitride.

While both PECVD and RPECVD have been studied and used for a number of years, the important reactions occurring in the plasma and plasma afterglow are not well understood. This lack of understanding hampers efforts to improve the efficiency and purity of silicon nitride coating processes.

Several groups have suggested that atomic nitrogen is of prime importance in the dissociation of silane.^{4,5} Indeed, one study has shown that the extent of silane decomposition in the active nitrogen scaled linearly with the number density of nitrogen atoms in the active nitrogen flow.⁶ Atomic nitrogen cannot be the only species controlling silane decomposition because the reaction between nitrogen atoms and silane is endoergic by about half of an electron volt.⁷ Furthermore we have shown⁸ that the rate coefficient for the reaction between atomic nitrogen and silane is insignificant ($k < 8 \times 10^{-14} \text{ cm}^3 \text{ molecule}^{-1} \text{ s}^{-1}$). The reactions of nitrogen atoms with SiH_x radicals with $x \leq 3$ are exoergic and undoubtedly do contribute to the overall decomposition of silane. Some species other than atomic nitrogen, however, must be responsible for the initial decomposition step.

While some investigators think that vibrationally excited nitrogen is crucially important in the initial decomposition step^{6,8}, several other research groups have concluded that vibrationally excited nitrogen does not appear to be important in the silane decomposition process.^{4,5,9}

Vibrationally excited nitrogen could contribute to silane dissociation in two different ways. In both paths the excited nitrogen would transfer several quanta of vibrational energy to the ν_1 or ν_3 modes of silane,



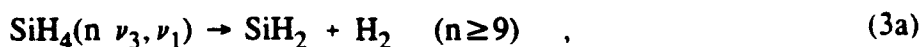
These two modes of silane are essentially resonant (within one kT) for one quantum transfers from nitrogen molecules that are excited as high as the fifteenth vibrational level (~ 4 eV). Since resonant energy transfer processes generally proceed facily this vibrational energy transfer process should be efficient.

The transfer of two quanta from $\text{N}_2(\nu)$ to SiH_4 is sufficient to render the reaction between ground-state nitrogen atoms and silane exoergic,

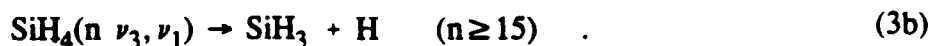


The SiH_x fragments can then be decomposed further in a series of N-atom reactions similar to reaction 2.

The other possibility is for the nitrogen to transfer vibrational energy to the silane until the silane obtains enough internal energy to dissociate unimolecularly,

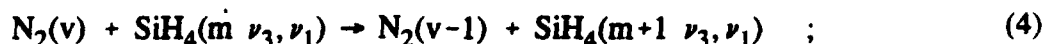


or

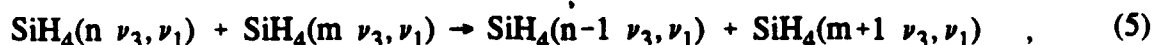


The SiH_4 decomposition would require at least nine quanta of nitrogen vibrational energy to effect the lowest energy decomposition step, that into SiH_2 and H_2 . If reaction 3b is the preferred decomposition pathway, 15 $\text{N}_2(\text{X}, \nu)$ quanta will be required. The two branches can be distinguished rather easily because reaction 3b will produce atomic hydrogen, whereas reaction 3a will not. Vacuum ultraviolet resonance fluorescence measurements provide a simple yet sensitive diagnostic for hydrogen atoms.

The vibrational pumping of the silane could proceed directly from a series of energy transfer collisions between the vibrationally excited nitrogen and the silane,



alternatively a number of energy pooling reactions between vibrationally excited silane molecules could occur:



where $m > n$.

O'Keefe and Lampe invoked energy-pooling processes to explain their observations of silane decomposition in mixtures of SiF_4 and SiH_4 that had been irradiated by a CO_2 laser at wavelengths that are absorbed only by the SiF_4 .¹⁰ They inferred that the laser irradiation resulted in vibrational excitation of the SiF_4 , which subsequently transferred its energy to the SiH_4 . The vibrationally excited SiH_4 then participated in a number of energy pooling collisions that ultimately led to decomposition into SiH_2 and H_2 . There was no decomposition of the SiF_4 , only the SiH_4 .

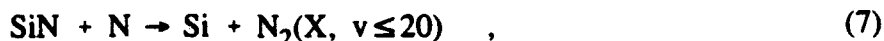
The temporal behavior of the decomposition following a laser pulse was quite interesting. Although the laser pulse lasted only about 2 μs , silane decomposition continued for roughly a millisecond. The decomposition rate reached a peak about 200 μs after the laser pulse and then decayed with a lifetime of approximately 300 μs . The most intriguing feature is that the decomposition process appeared to have an incubation period. The rate of decomposition was an order of magnitude greater during the second 100 μs than during the first 100 μs following the laser pulse.

The incubation period prior to rapid silane decomposition that O'Keefe and Lamp noted is reminiscent of observations in two recent flowing afterglow studies on the decomposition of silane in active nitrogen.^{6,9} Both studies noted an incubation period prior to silane decomposition. Horie et al.⁹ observed that both silane and atomic nitrogen number densities remained relatively constant over periods of time up to 35 ms, depending upon the ratio of initial number densities of atomic nitrogen to silane, and then decreased fairly rapidly after this incubation period. For example, under one set of conditions that they investigated, the silane and N-atom number densities decreased very little for more than 20 ms after the silane and active nitrogen had been mixed. During the next 6 to 8 ms, however, the silane and the N atoms were consumed completely. This peculiar behavior could be explained if something like 20 ms were required for nitrogen to couple adequate internal energy to the silane before it could decompose. Then once the decomposition was begun, its rate could accelerate rapidly if some reaction chain continued further decomposition.

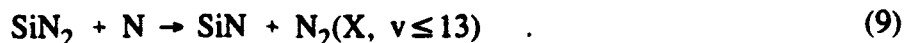
DeJoseph proposed a mechanism that gave an alternative explanation to the incubation time.⁶ He postulated that the primary reaction necessary to begin silane decomposition was,



The SiH_2 was then further decomposed by reactions with nitrogen atoms. The novel idea in this postulated decomposition mechanism was a series of three reactions that regenerated the $\text{N}_2(\text{v})$:



and



The net effect of these three reactions is to generate two $\text{N}_2(\text{v})$ molecules in the recombination of two N atoms. As the reaction progresses, therefore, the number density of the $\text{N}_2(\text{X}, \text{v} \geq 10)$ builds up and this build up accelerates the rate of silane decomposition. With this set of reactions at its core, DeJoseph constructed a kinetic model for silane decomposition that reproduced moderately well the temporal observations of Horie et al. using a reasonable set of rate coefficients.

The basic mechanism for silane decomposition described by reactions 6 to 9 can be distinguished experimentally from that which incorporates reactions 1 to 5 because the temporal variation of the number densities of $\text{N}_2(\text{X}, \text{v} \geq 10)$ will differ dramatically between the two models. The first mechanism, reaction 1 to 5, will have the $\text{N}_2(\text{X}, \text{v} \geq 10)$ number densities diminish over time. Expectations based upon the second mechanism, reaction 6 to 9, on the other hand, are that the $\text{N}_2(\text{X}, \text{v} \geq 10)$ number densities will increase by several orders of magnitude over time. Identifying the correct mechanism requires a diagnostic for vibrational levels of ground-state nitrogen greater than ten. We developed this capability recently during a course of investigations on the kinetics of $\text{N}_2(\text{X}, \text{v})$ in prospective chemical laser systems.^{11,12}

The basic goals of this program were to try to determine the importance vibrationally excited nitrogen plays in silane decomposition in silicon nitride coating systems. Our primary focus was on characterizing the reactions between $\text{N}_2(\text{X}, \text{v})$ and SiH_4 . To this end we studied the kinetics of $\text{N}_2(\text{X}, \text{v})$ quenching by SiH_4 in some detail. In addition to determining rate coefficients as a function of vibrational level, we showed that the quenching process can be characterized as a series of single-quantum transfers and that one channel for the reaction is $\text{SiH}_4(\nu_3)$ excitation.

We also began a series of experiments aimed at forming silicon nitride coatings on single-crystal substrates. Although these experiments were limited in extent, successful coatings were generated with little difficulty. In addition silicon nitride powder was also formed in these experiments.

3. EXPERIMENTAL

The experiments were all done in a discharge-flow reactor. Different configurations were used depending upon the effects being studied. The bulk of the experiments, designed to measure rate coefficients for $N_2(X, v)$ removal by SiH_4 , used the apparatus shown schematically in Figure 1. It consists of a 4.6-cm i.d. quartz tube, 50 cm long. $N_2(X, v)$ is injected into the upstream end of the reactor, and is detected at the downstream end by monitoring fluorescence excited by the interaction of $N_2(X, v)$ with either $N_2(A)$ or $He(2^3S)$. A loop injector that can be moved along the length of the reactor mixes silane with $N_2(X, v)$. The flow reactor was pumped by a roots blower/forepump combination capable of producing flow velocities of 5×10^3 cm s⁻¹ at a pressure of 1 Torr. Generally much more modest flow velocities were required and the flow reactor access to the pump was throttled by a downstream butterfly valve.

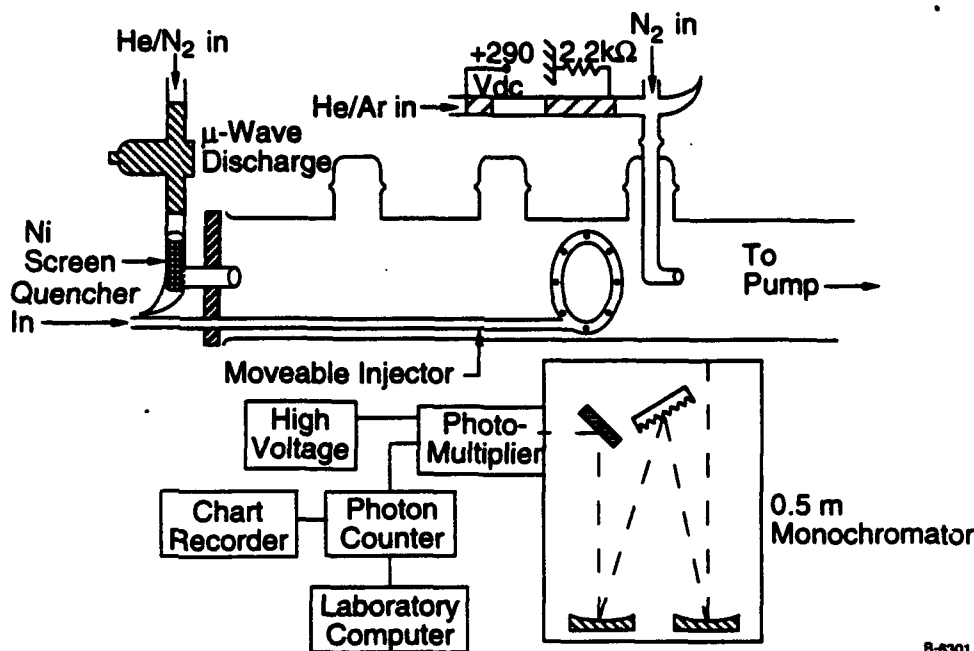


Figure 1. Discharge flow reactor for studying the kinetics of reactions involving $N_2(X, v)$

$N_2(X, v)$ is prepared in a microwave discharge through a mixture of nitrogen dilute in helium. The effluents of the discharged mixture then pass through a nickel screen prior to their entry into the flow reactor. The screen removes the atoms and deactivates electronically excited metastables, but has relatively little effect on vibrationally excited N_2 . Our previous observations¹³ indicate that the Ni screen reduces N atom number densities about a factor of 50, to a level of about 1×10^{11} cm³ molecule⁻¹ s⁻¹. This reduction is, of course, dependent to some extent upon the screen mesh and contact time between the discharge effluents and the screen. In our experiments the screen is about 24 mesh and consists of two coaxial cylinders about 5 cm long inserted into the 12.7-mm o.d. discharge

tube downstream from the discharge. They cover the opening in the side of the discharge tube through which the effluents must pass to enter the flow reactor.

Metastable $\text{He}(2^3\text{S})$ and $\text{N}_2(\text{A})$ enter the flow reactor through a 10 cm o.d. hook-shaped injector inserted into the flow reactor at its downstream end. The metastables are generated in the upstream end of the injector and emanate from the injector along the flow reactor axis. A hollow cathode, dc discharge, biased at 290V dc, generates $\text{He}(2^3\text{S})$ if the injector flow is pure helium, or metastable $\text{Ar}(^3\text{P}_{0,2})$ if a few percent argon is added to the helium flow. The metastable argon is used to produce the $\text{N}_2(\text{A})$ metastables by excitation transfer.¹⁴ In this case, nitrogen is added in the injector just downstream from the discharge cathode. The lack of emission from $\text{N}_2^+(\text{C})$ or $\text{N}_2^+(\text{B}, v \geq 2)$ when the He metastables are added to cold N_2 shows that both He^+ and He_2^+ are absent from the flow of metastables entering the flow reactor.¹⁵

Gas flow rates are measured by electronic mass flow meters, or in a few instances by rotameters, that have been calibrated by measuring the rates of pressure increase as a function of time when gases flow into a calibrated volume. Because some of our initial results were puzzling, the mass flow meters, were extensively recalibrated. The only significant change from this procedure was that the SiH_4 calibration was about 15% less than we had anticipated based upon the flow meter calibration with argon and the standard correction procedure involving the ratio of gas specific heats. Capacitance manometers measured the flow reactor pressures.

A 0.5-m monochromator, sensitive to radiation between 200 and 900 nm, detected radiation in the flow reactor: the N_2 first-negative bands, $\text{N}_2^+(\text{B } ^2\Sigma^+ - \text{X } ^2\Sigma^+)$ between 350 and 500 nm, from the $\text{He}^*(2^3\text{S})/\text{N}_2(\text{X}, v \leq 6)$ interaction; the N_2 first-positive bands, $\text{N}_2(\text{B } ^3\Pi_g - \text{A } ^3\Sigma_u^+)$ between 560 and 900 nm, from the $\text{N}_2(\text{A } ^3\Sigma_u^+)/\text{N}_2(\text{X}, v \geq 5)$ interaction; and the N_2 Vegard-Kaplan bands, $\text{N}_2(\text{A } ^3\Sigma_u^+ - \text{X } ^1\Sigma_g^+)$ between 250 and 400 nm, diagnostic of $\text{N}_2(\text{A})$ number densities. The monochromator had a 1200 groove mm^{-1} grating blazed at 250 nm and a thermoelectrically cooled photomultiplier. Signals from the photomultiplier were processed by either a photon-counting rate meter or a picoammeter. Their outputs were recorded by a strip-chart recorder and stored digitally by a lab computer system. A least-squares, spectral fitting procedure, described in some detail previously, determined band intensities from the spectra.¹⁶

Another set of experiments used the apparatus shown schematically in Figure 2. These experiments were designed to monitor infrared fluorescence from SiH_4 excited by vibration-vibration exchange from $\text{N}_2(\text{X}, v)$. For these experiments a 5-cm i.d. flow tube was configured to allow spectral observations along the axis of the flow reactor. The upstream end of the flow reactor was sealed with a CaF_2 window and placed directly in front of the monochromator slit. The effective field of view was about 32 cm long. Generally the $\text{N}_2(\text{X}, v)$ entered directly in front of the window, normal to the axis of the field of view. Silane, or in some cases nitrous oxide, was added through a loop injector situated directly in front of the window. In some experiments, the $\text{N}_2(\text{X}, v)$ and silane flowed through a 50-cm

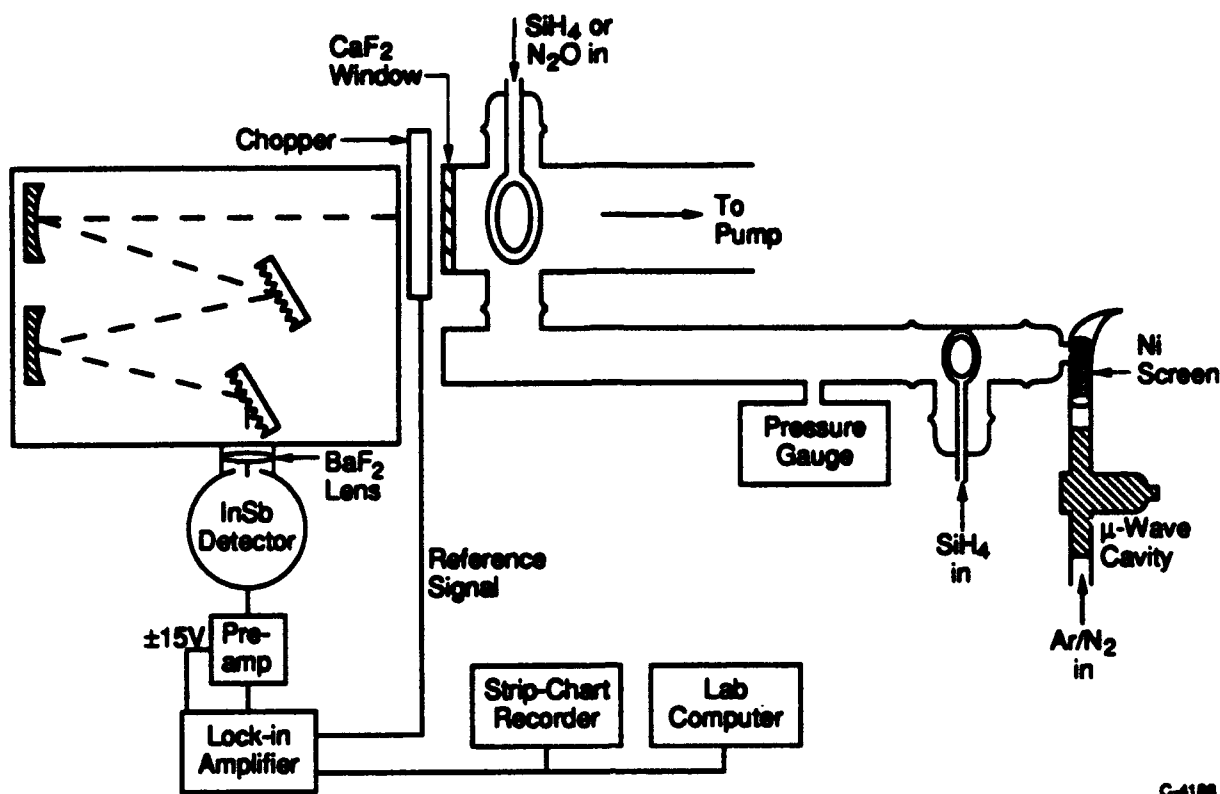


Figure 2. Schematic of apparatus for observing $\text{SiH}_4(\nu_3)$ infrared emission

long, 2.5-cm i.d. side arm before entering the 5-cm tube within the monochromator field of view.

Most infrared spectral observations were made between 2000 and 5000 nm using the 0.5-m monochromator equipped with a $150 \text{ groove mm}^{-1}$ grating blazed at 3000 nm and a liquid nitrogen cooled InSb detector. In a few cases a $300 \text{ groove mm}^{-1}$ grating blazed at 1000 nm and a liquid nitrogen cooled intrinsic Ge detector were used with the monochromator to allow the spectral region between 1000 and 1600 nm to be monitored. In both cases, light from the observation region was chopped prior to entering the monochromator and signals from the detectors were processed with a phase-sensitive amplifier. The output from the lock-in amplifier was recorded by a strip-chart recorder and, in addition, stored digitally in a computer file.

A third set of experiments were directed at coating several substrates with silicon nitride films. These experiments used a different 5 cm diameter, quartz flow reactor, illustrated schematically in Figure 3. It was pumped by a rotary mechanical pump. Active nitrogen was generated at the upstream end of the flow reactor in a microwave discharge of nitrogen dilute in argon. Silane was injected through a loop injector whose position could be varied along the length of the reactor, and the active nitrogen, silane mixture impinged upon a substrate mounted on a copper cap on the end of a rod heater. Some initial experiments

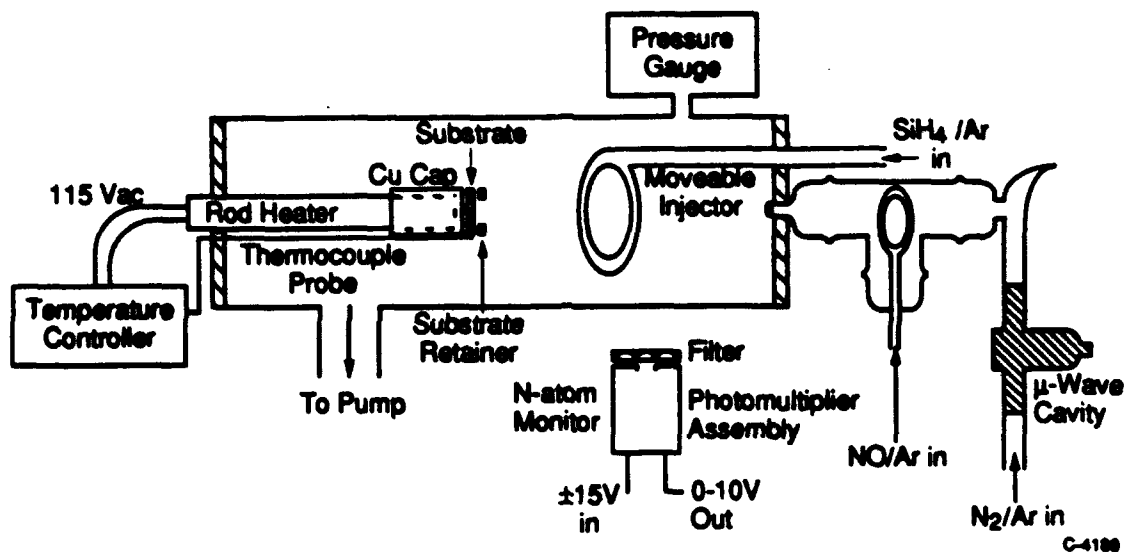
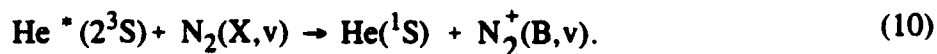


Figure 3. Schematic of apparatus for coating substrates with silicon nitride

used sapphire substrates, but later experiments used fragments of single crystal silicon wafers, polished on both sides. The substrate was sandwiched between the cap on the rod heater and a copper ring that was screwed into the cap. In addition a thermocouple was wedged under the copper retainer. The output of the thermocouple was wired to a commercial temperature controller. As in all other experiments, flow rates were monitored by electronic mass flow meters. We found it necessary to use a mass flow controller to maintain a constant flow of silane. The other gas flows remained constant so long as their gas cylinder delivery pressures and needle valve settings remained constant. The pressure in this reactor was measured with a capacitance manometer. Typical conditions included flow rates of argon carrier gas and nitrogen of 880 and 90 micromoles s^{-1} , respectively, and a total pressure of 3 Torr.

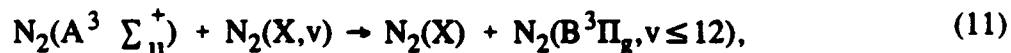
4. ENERGY-TRANSFER BASED DIAGNOSTICS OF $N_2(X, v)$

We have developed techniques recently for determining number densities of vibrationally excited nitrogen in vibrational levels up through about fifteen.^{11,12,17-20} Two different methods are used to probe different ranges of vibrational excitation. The first, which gives absolute $N_2(X, v)$ number densities for vibrational levels up through about six, involves measuring the vibrational distribution of the nitrogen first-negative bands when they are excited in the Penning-ionization reaction between metastable helium atoms and $N_2(X, v)$,



The ground-electronic-state vibrational distribution of nitrogen can be deduced from the $N_2^+(B)$ vibrational distribution and the Franck-Condon factors that connect the ground electronic state of the neutral molecule to the electronically excited state of the molecular ion (vide infra).^{12,17,18}

The second $N_2(X, v)$ diagnostic gives semi-quantitative estimates of $N_2(X, v)$ number densities for vibrational levels greater than 4 (about 5 to 15).^{11,19,20} Metastable nitrogen molecules, $N_2(A^3\Sigma_u^+)$, excite $N_2(X, v \sim 5-15)$ to $N_2(B, v \leq 12)$ quite efficiently,



where $k_2 \sim 4 \times 10^{-11} \text{ cm}^3 \text{ molecules}^{-1} \text{ s}^{-1}$. Measurements of the intensity and vibrational distribution of the $N_2(B)$ fluorescence in the presence of known amounts of $N_2(A)$ will give the number densities of these highly excited levels of $N_2(X, v)$ to within factors of two to three. Relative variations in $N_2(X, v)$ number densities can be determined to within about 20%.

We have employed the second $N_2(X, v)$ diagnostic to determine rate coefficients for vibrational energy transfer from $N_2(X, v)$ to a number of other molecules.¹⁹ The technique involves comparing the $N_2(B)$ intensities from $N_2(A)$ excitation of $N_2(X, v)$ between conditions under which the mixing time of the quencher and the vibrationally excited nitrogen is quite short, 2 to 3 ms, and conditions under which the contact time is much longer, 20 to 40 ms. This approach allows one to distinguish between reductions in $N_2(B)$ intensity caused by electronic quenching of $N_2(B)$ from those resulting from a reduction in the $N_2(X, v)$ number density.

These measurements use a relatively clean source of $N_2(X, v)$, one that is essentially free from accompanying atomic nitrogen or electronically excited metastables. This source involves passing the effluents from a discharge, in a mixture of nitrogen in helium, through a

nickel screen. The nickel screen reduces atomic nitrogen number densities in the afterglow by factors of 50 or more, but attenuates the $N_2(X, v)$ very little.^{13,18}

4.1 Penning Ionization

Our Penning-Ionization diagnostic for vibrationally excited nitrogen in discharge afterglows follows along the lines of the pioneering work of Schmeltekopf et al.²¹ and Young and Horn.^{22,23} Mixing metastable helium atoms with a flow of molecular nitrogen results in strong emission of the nitrogen first-negative system, $N_2^+(B^2\Sigma_u^+ - X^2\Sigma_g^+)$. Since the Penning-Ionization process follows a Franck-Condon excitation pathway, the vibrational distribution in the neutral, ground state will determine the distribution observed in the upper, ionic state. One problem with this approach is that care must be taken not to have any He^+ or He_2^+ in the flow of metastable helium. Both of those species also excite $N_2^+(B)$ quite strongly in charge-transfer reactions, but with an $N_2^+(B)$ vibrational distribution that is decidedly non-Franck-Condon.¹⁵ We have been careful to eliminate ions in our system.

The rate of Penning-ionization between metastable helium atoms and molecular nitrogen is proportional to the Franck-Condon factors that connect the $N_2^+(B)$ and $N_2(X)$ states. One can calculate the vibrational distribution in the final state, therefore, knowing only the vibrational distribution in the lower state and the Franck-Condon factors that couple the two states. Thus,

$$N_{v'} \propto \sum_{v''} N_{v''} q_{v'v''} \quad (12)$$

where v' and v'' represent the vibrational levels of the upper and lower states, respectively, and $q_{v'v''}$ is the Franck-Condon factor coupling them. We have calculated a comprehensive set of Franck-Condon factors for $N_2^+(B) - N_2(X)$ transitions, and have tabulated them elsewhere.²⁴

We determine relative $N_2(X, v)$ distributions by finding the model distribution that can be used in Eq. (12) to predict $N_2^+(B)$ vibrational distributions that are most like those observed experimentally. The $N_2(X, v)$ vibrational distributions usually follow a modified Treanor²⁵⁻²⁷ model, which simplifies the fitting process. We do have fitting procedures, however, to determine populations for cases for which the Treanor model is inapplicable.^{12,18}

The modified Treanor distribution has been outlined by Caledonia and Center,²⁶ and Dilonardo and Capitelli.²⁷ For low vibrational levels the distribution is that given by Treanor et al.:²⁵

$$\frac{N_{v''}}{N_{v''=0}} = \exp \left[-v'' \left[\frac{1.4388 (\omega_e - 2\omega_e x_e)}{\Theta_1} - (v'' - 1) \frac{1.4388 \omega_e x_e}{T} \right] \right], \quad (13)$$

where Θ_1 is the Boltzmann vibrational temperature referenced to $v'' = 1$, T is the ambient gas translational temperature, and ω_e and $\omega_e x_e$ are spectroscopic constants in units of cm^{-1} . The Boltzmann vibrational temperature is given by

$$\Theta_1 = -\frac{\omega_e - 2\omega_e x_e}{k \ln(N_{v''=1}/N_{v''=0})}, \quad (14)$$

where k is Boltzmann's constant.

This distribution goes through a minimum, called the Treanor minimum, at v^* , given by

$$v^* = \frac{T(\omega_e - 2\omega_e x_e)}{2\omega_e x_e \Theta_1} + 0.5 \quad (15)$$

For vibrational levels above the Treanor minimum, the Product vN_v is essentially constant.²⁶ The resulting distribution for $v > v^*$ is

$$\frac{N_{v''}}{N_{v''=0}} = \frac{(v^* - 1) \exp(-1.4388(v^{*2} - 1)\omega_e x_e/T)}{v}, \quad (16)$$

where the various parameters in Eq. (16) are determined by requiring the two distributions, i.e., Eqs. (13) and (16), be equal at v'' and $v^* - 1$. Rather than use an explicit Θ_1 value, we base our distributions on an effective Θ_1 which best fits all the data points.

Fitting the Penning-ionization spectra to a ground-state vibrational model, as just described, gives only the relative distribution among ground-state vibrational levels. We place this relative distribution on an absolute basis, however, by determining the absolute number density of $N_2(X, v''=0)$. This is accomplished by noting changes in intensity of $N_2^+(B, v' = 0, 1)$ when the $N_2(X, v)$ producing discharge is struck relative to the intensities when the discharge is off. We know, of course, the absolute $N_2(X, v''=0)$ number density when the discharge is off.

4.2 $N_2(A)$ Energy Transfer

The Penning-ionization diagnostic is inadequate for studies on $N_2(X, v'' \geq 6)$ as discussed earlier. To overcome this problem we developed a semiquantitative technique for determining number densities of $N_2(X, v'' \geq 5)$. Our diagnostic method for monitoring $N_2(X, v'' \geq 5)$ is based upon measuring nitrogen first-positive emission intensities excited in the reaction between $N_2(A)$ and $N_2(X, v'')$. These intensities are directly proportional to $N_2(X, v'')$ number densities. The observed intensities must be corrected for any quenching of the first-positive emission before they can be related to $N_2(X, v'')$ number densities.

The intensity of the N_2 first-positive emission is given by

$$I = k_r[N_2(B)] = \frac{k_{11}[N_2(X, v'')][N_2(A)]}{1 + \sum_i \frac{k_{Qi}[Q_i]}{k_r}} \quad (17)$$

where k_{Qi} is the rate coefficient for $N_2(B)$ quenching by quenchers Q_i and k_r is the $N_2(B)$ radiative decay rate.¹⁶ The buffer gas pressure, primarily helium is ≤ 1 torr. This minimizes quenching by the bath gas species in the flow tube.²⁸ Rearranging Eq. (17) gives

$$[N_2(X, v'')] = \frac{k_r[N_2(B)]}{k_{11}[N_2(A)]} \left\{ 1 + \sum_i \frac{k_{Qi}[Q_i]}{k_r} \right\} \quad (18)$$

While determining absolute values for $[N_2(A)]$ or $[N_2(B)]$ is difficult and therefore quite uncertain, measuring the ratio of these two number densities accurately is straightforward because only relative sensitivities of the detection system at the various wavelengths are required.

Although primarily a global monitor of $N_2(X, v'')$, this diagnostic does provide some state specificity. The higher vibronic levels of $N_2(B)$ are accessible only from $N_2(X, v'')$ vibrational levels at the high end of the diagnostic range. For example $N_2(B, v'=10)$ can be excited only from $N_2(X, v'' \geq 12)$. Thus, we track the varying behavior of $N_2(X, v'' \geq 12)$ by measuring $N_2(B, v=10)$ intensities.

5. N₂(X, v) QUENCHING BY SiH₄

5.1 Experimental Approach

Because our diagnostic techniques involve adding metastables to the flow reactor and observing the fluorescence excited when the metastable interacts with SiH₄, we need to separate diminutions in the observed fluorescence caused by fluorescence or metastable quenching from the diminutions resulting from removal of N₂(X, v) from the reactor. We separate these effects by varying the mixing time between the N₂(X, v) and the SiH₄ over a wide range.

When quencher is injected immediately behind the N₂(A) (or He*) inlet, the number density of N₂(X, v") remains essentially unchanged. This is because vibrational quenching is a relatively slow process ($k_v \leq 10^{-14} \text{ cm}^3 \text{ molecule}^{-1} \text{ s}^{-1}$) and reagents are mixed for too short of time ($\leq 2 \text{ ms}$) to effect significant quenching. Any diminution in the first-positive (negative) emission, therefore, results from quenching of N₂(B) (N₂⁺(B)), or perhaps N₂(A) (He*). Injecting the reagent at the upstream end of the flow reactor allows adequate time (~ 10 to 30 ms) for the N₂(X, v") to be quenched unless the quenching rate coefficients are exceedingly small. Any difference in diminution of the first-positive (negative) emission with the injector in the upstream position as compared to the downstream position can be attributed to quenching of N₂(X, v") by the added reagent.

Figure 4 illustrates these concepts. It shows a portion of the spectrum of N₂(B-A) emission, excited by the reaction between N₂(A) and N₂(X, v), in the absence of any added quencher and in the presence of a fixed concentration of a SiH₄ at a small mixing time, and one 21.7 ms greater. Adding the SiH₄ at the short time drops the N₂(B-A) emission about a factor of 1.6. When the mixing time is increased by 21.7 ms, the first-positive emission intensity diminishes almost another factor of 1.6. We can estimate rate coefficients for N₂(X, v) and N₂(B, v) quenching by SiH₄ from these data as shown below.

In the absence of added quencher, the intensity of the N₂ first-positive emission is given by¹¹

$$I_0 = k_r[N_2(B)] = k_{11}[N_2(X, v'')][N_2(A)] \quad (19)$$

For global measurements, k_r , the radiative decay rate of the N₂(B),¹⁶ is about $1.5 \times 10^5 \text{ s}^{-1}$. The experiments use a helium bath-gas at pressures of about 1 Torr. This reduces quenching in the flow tube to less than a 20% effect.²⁸ As a result we neglect bath-gas quenching in Eq. (19).

Then the quencher is introduced into the flow reactor with the injector in the downstream position, that is short interaction times where N₂(X, v) removal is negligible, the first-positive emission intensity is given by

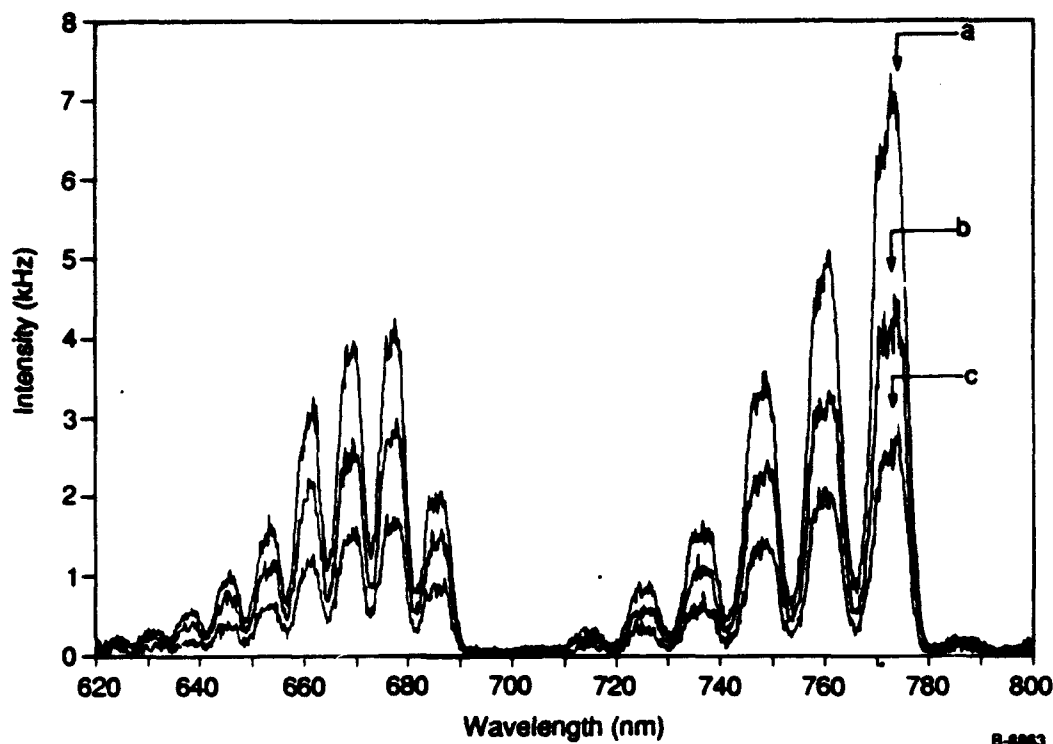


Figure 4. Variation in the $N_2(B-A)$ intensity excited in the $N_2(A) + N_2(X,v)$ reaction, as a function of reaction time and SiH_4 number density. Conditions in the order of decreasing intensity are: a) $SiH_4 = 0$, $\Delta t = 0$ ms; b) $SiH_4 = 2.3 \times 10^{13}$ molecules cm^{-3} , $\Delta t = 0$ ms; c) $SiH_4 = 2.3 \times 10^{13}$ molecules cm^{-3} , $\Delta t = 21.7$ ms.

$$I = k_r[N_2(B)] = \frac{k_{11}[N_2(A)][N_2(X,v'')]}{1 + \frac{k_Q[Q]}{k_r}}, \quad (20)$$

where k_Q is the rate coefficient for $N_2(B)$ quenching by SiH_4 . $N_2(A)$ number densities are also measured under each set of conditions to correct any quenching of the $N_2(A)$. Taking the ratio of the first-positive intensity in the absence of quencher to that in the presence of quencher gives the classical Stern-Volmer formula²⁹ for electronic quenching, viz.,

$$\Gamma = \frac{I_o/[N_2A]_o}{I/[N_2A]} = 1 + k_Q[Q]/k_r, \quad (21)$$

where the subscript o refers to conditions in the absence of added quencher. The rate coefficient for $N_2(B)$ quenching for data taken with the injector in the downstream position is,

$$k_Q = \frac{k_r}{[Q]} \{\Gamma - 1\}. \quad (22)$$

With the injector in the upstream position, the $N_2(X, v'')$ is also quenched and the first-positive emission intensity is described by

$$I = k_r [N_2(B)] = \frac{k_{11} [N_2(X, v'')]_0 e^{-k_v [Q] \Delta t}}{1 + \frac{k_Q [Q]}{k_r}}, \quad (23)$$

where k_v is the rate coefficient for $N_2(X, v'')$ quenching and Δt is the time the quencher and the $N_2(X, v'')$ are mixed. The $N_2(X, v'')$ quenching rate coefficient is determined from the slope of the natural log of the ratio to Stern-Volmer factors at long to short decay times plotted against $[Q]\Delta t$, i.e.,

$$\ln(\Gamma_u/\Gamma_d) = k_v [Q] \Delta t, \quad (24)$$

where the subscripts u and d refer to measurements with the injector in the upstream and downstream positions, respectively.

5.2 Results for $N_2(X, v \geq 5)$

Figures 5 to 7 are representative plots of the data, and Table 1 summarizes all results from the studies using the $N_2(A)$ energy transfer diagnostic. Since rate coefficients for electronic quenching of $N_2(B)$ necessarily are determined in the data analysis, they are also listed in Table 1. The error bars represent one standard deviation of the slopes when data are plotted according to Eq. (24).

The vibrational relaxation rate coefficients determined by the Eq. (24) analysis should properly be taken to be lower limits to the true vibrational relaxation rate coefficients. Since the ν_3 mode of SiH_4 is resonant to within kT for single quantum transfer from $N_2(X, v)$, the mechanism for the relaxation most likely proceeds one step at a time. Thus the actual process being measured will be the net difference between relaxation of all vibrational levels above a given level into that level and the removal of vibrational energy from the given level into all vibrational levels below it. Even so, the lower-limit vibrational relaxation rate coefficients are quite large, being about twice the size of the rate coefficient for quenching $N_2(X, v)$ by N_2O and an order of magnitude or more greater than the rate coefficients for vibrational relaxation by CO , CO_2 , and N_2 ,¹⁹ species that are generally considered to be effective at removing vibrational energy from $N_2(X, v)$.

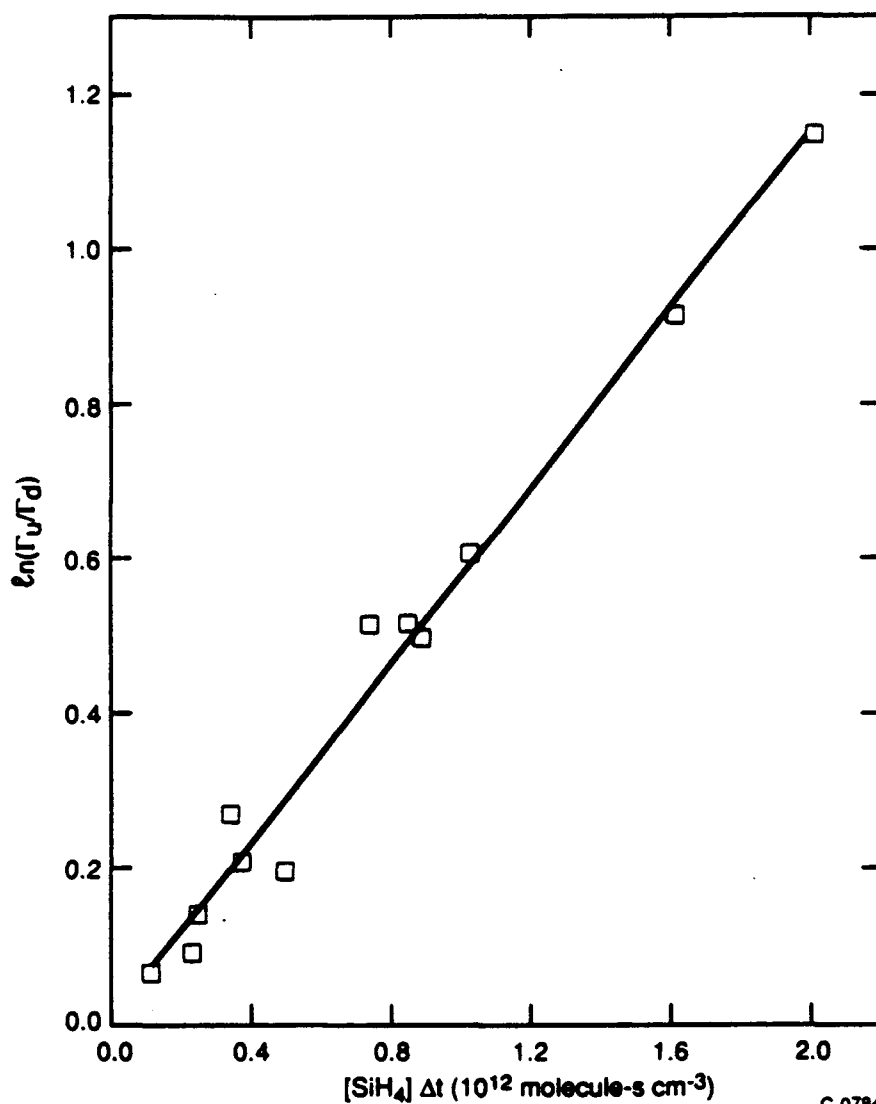


Figure 5. Net quenching of $\text{N}_2(\text{X}, v \geq 6)$ by silane

The rate coefficients for electronic quenching of $\text{N}_2(\text{B})$ seemed unusually large and caused some concern as to the validity of our measurements. Since the primary measurement is of the ratio of two intensities, calibration of the optical system will not contribute to possible errors in the rate coefficients. The other two measured quantities, $[\text{SiH}_4]$ and Δt , both depend primarily on gas flow rate measurements. Consequently we did an extensive set of calibrations of our flow meters. These calibrations involved measuring the increase of pressure in a calibrated volume as a function of time. We used two different volumes that we calibrated in situ by comparison with a flask whose volume had been determined previously by measuring the difference between its weight with the flask filled with water and with it empty. In addition we used two different pressure transducers for the pressure measurements. The results of these measurements showed good agreement both with previous calibrations and with manufacturer's specifications for a number different gases and flow meters. The calibration for the SiH_4 flow meter was tested against Ar, N_2 , CH_4 ,

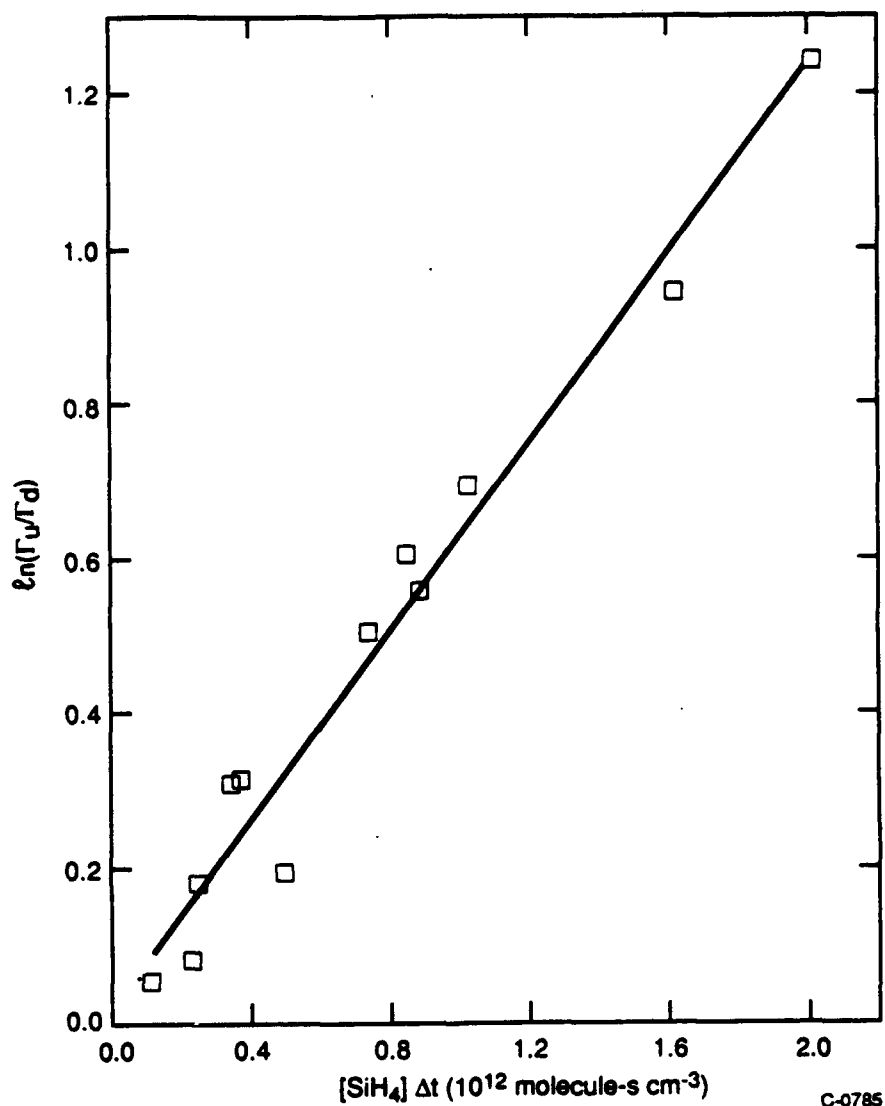


Figure 6. Net quenching of $N_2(X, v \geq 9)$ by SiH_4

N_2O , and SF_6 in addition to SiH_4 . With the exception of SiH_4 , the calibrations were within 5% of manufacturer's specifications. At the low end of its range, the SiH_4 flow meter read about 15% below specifications. At the top end of the flow meter range the discrepancy was only 2%.

We also considered the effects of $N_2(X, v)$ quenching during the short transit time from the SiH_4 injector to the observation region when the injector was in the downstream position. This correction generally amounted to no more than 10 to 20%. Finally, we have used this same technique to measure rate coefficients for $N_2(B)$ quenching by a variety of other gases with reasonable agreement between our results and those of other groups who used different measurement techniques.¹⁹ It appears, therefore, that silane quenches $N_2(B)$ with remarkable efficiency. The attractive forces between the two molecules are sufficiently

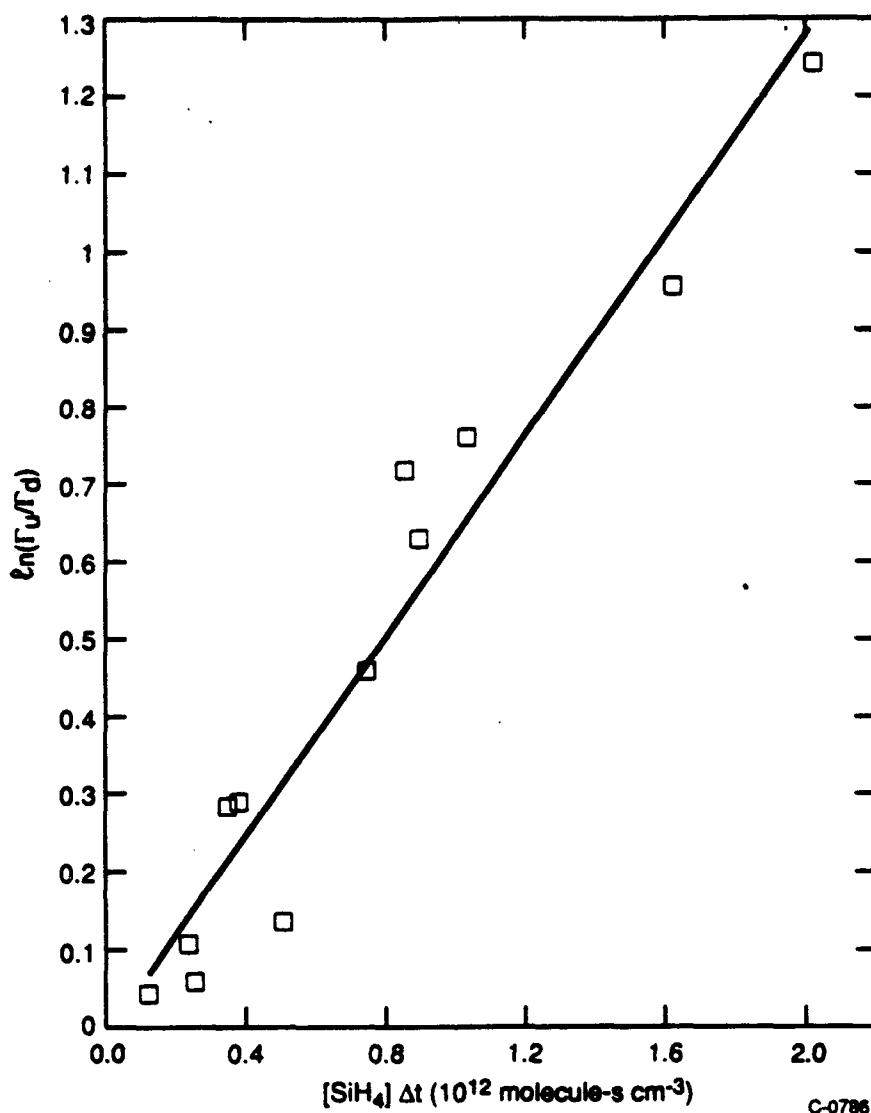


Figure 7. Net quenching by $N_2(X, v \geq 11)$ by SiH_4

strong that quenching takes place at a rate significantly greater than the hard-sphere collision rate.

5.3 Results for $N_2(X, v \leq 6)$

An analysis of the variations in the number densities of $N_2(X, v < 6)$, determined from the He^+ Penning-ionization diagnostic, as a function of the product $[SiH_4]\Delta t$, i.e., equivalent to the analysis related to Eq. (24), gives plots such as Figures 8 and 9 and the set of rate coefficients given in the second column of Table 2. As in the results in Table 1, these values can only properly be considered lower limits.

Because the Penning-ionization diagnostic provides absolute number densities of molecules in each vibrational level, these data are amenable to an alternative analysis that

Table 1. Rate Coefficients for $N_2(X, v)$ and $N_2(B^3\Pi_g)$ Quenching by SiH_4

$N_2(X, v)$		$N_2(B, v)$	
Vibrational Levels	Rate Coefficient ($10^{-13} \text{ cm}^3 \text{ molecule}^{-1} \text{ s}^{-1}$)	Vibrational Levels	Rate Coefficient ($10^{-9} \text{ cm}^3 \text{ molecule}^{-1} \text{ s}^{-1}$)
≥ 5	4.1 ± 0.5	1	2.2 ± 0.5
≥ 6	5.7 ± 0.3	2	2.7 ± 0.6
≥ 7	5.3 ± 0.4	3	2.2 ± 0.5
≥ 8	5.7 ± 0.3	4	2.2 ± 0.7
≥ 8	5.9 ± 0.4	5	2.8 ± 0.8
≥ 9	6.0 ± 0.4	6	2.9 ± 0.9
≥ 10	5.9 ± 0.5	7	2.9 ± 1.2
≥ 11	5.5 ± 0.6	8	3.4 ± 0.9
≥ 11	6.4 ± 0.5	9	3.4 ± 0.8
≥ 12	5.1 ± 0.7	10	4.3 ± 1.3
≥ 13	5.2 ± 0.8	11	3.0 ± 0.8
≥ 13	4.9 ± 1.1	12	2.7 ± 1.7
Unweighted avg	5.5 ± 0.6	Unweighted avg	2.9 ± 0.6

incorporates the effects of single quantum transfer from a given level to the one below it. Although the form of our data set makes the single quantum analysis somewhat crude, the results are still enlightening.

The differential equation describing the time rate of change of molecules in level v with number density N_v is

$$\frac{dN_v}{dt} = k_{v+1}N_{v+1}[SiH_4] - k_vN_v[SiH_4] \quad (25)$$

where the first term on the right-hand side of the equation represents the rate of formation of level v from level $v+1$ above, and the second term represents the removal rate from level v into level $v-1$. Rearranging this equation and integrating it gives

$$\int dN_v = N_v - N_v^0 = k_{v+1}[SiH_4] \int N_{v+1}dt - k_v[SiH_4] \int N_vdt \quad (26)$$

An approximate value for the integral expressions on the right-hand side of Eq. (26) is

$$\int N_vdt \approx \frac{N_v^0 + N_v}{2} \Delta t \quad (27)$$

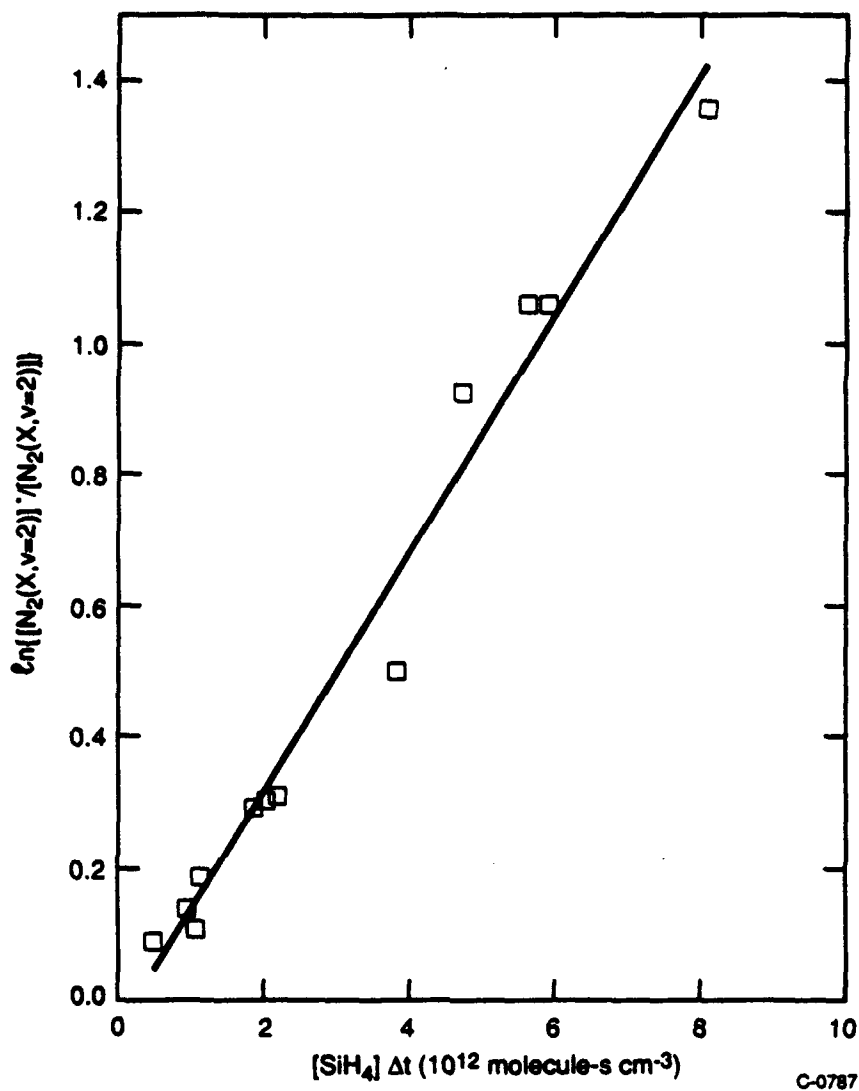


Figure 8. Net quenching of $N_2(X, v=2)$ by SiH_4

Thus we can rewrite Eq. (27) as

$$N_v - N_v^0 = k_{v+1} \left[\frac{N_{v+1}^0 + N_{v+1}}{2} \right] [SiH_4] \Delta t - k_v \left[\frac{N_v^0 + N_v}{2} \right] [SiH_4] \Delta t \quad (28)$$

Summing the equation from level v up to level v_{max} , the highest vibrational level observed, gives

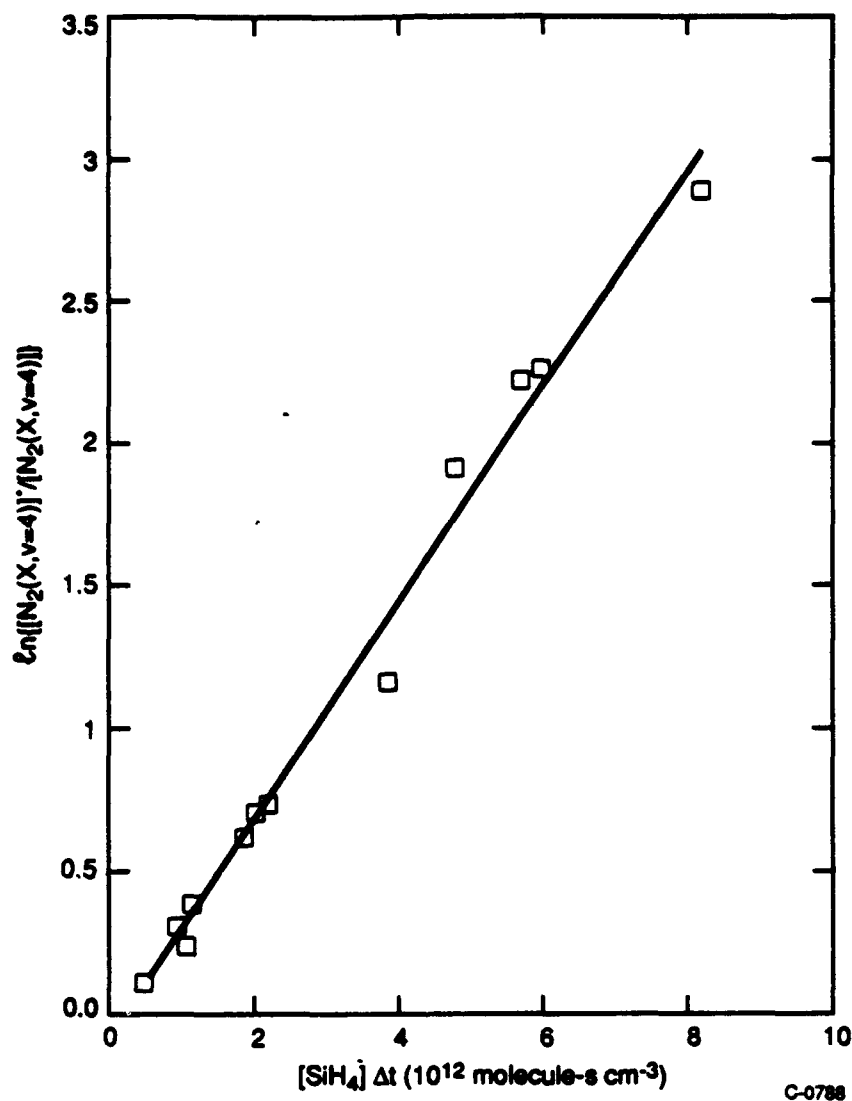


Figure 9. Net quenching of $N_2(X, v=4)$ by SiH_4

$$\sum_v^{v_{\max}} (N_v - N_v^0) = k_{v_{\max}} \left[\frac{N_{v_{\max}} + N_{v_{\max}}}{2} \right] [SiH_4] \Delta t \quad (29)$$

$$- k_v \left[\frac{N_v^0 + N_v}{2} \right] SiH_4 \Delta t$$

Since the vibrational population falls off fairly rapidly as v increases, the term in v_{\max} can be neglected compared to the term in v provided v is several quanta below v_{\max} . Thus after rearrangement we are left with a simple two term expression:

Table 2. Rate Coefficients for Relaxation of $N_2(X,v)$ Using Penning-ionization Diagnostic

Vibrational Level	Rate Coefficient ^a	
	Net Removal	Single Quantum Transfer Analysis
1	0.84 ± 0.05	1.3 ± 0.1
2	1.8 ± 0.1	2.6 ± 0.2
3	2.8 ± 0.1	3.6 ± 0.2
4	3.8 ± 0.1	6.0 ± 1.0
5	4.8 ± 0.2	6.0 ± 1.0
6	5.8 ± 0.2	4.5 ± 1.0
^a Rate Coefficients at 300 K in units of $10^{-13} \text{cm}^3 \text{molecule}^{-1} \text{s}^{-1}$		

$$2 \frac{\sum_{v=1}^{v_{\max}} N_v^0 - N_v}{N_v^0 + N_v} = k_v [\text{SiH}_4] \Delta t \quad (30)$$

What this equation says is that the number of molecules lost from level v is not just those determined from the direct change in the population of level v itself, but actually includes the sum of the population lost by all molecules in vibrational levels above v .

Figures 10 and 11 show some of our data plotted according to Eq. (30). The slopes of the lines in these plots give the value of the vibrational relaxation rate coefficients. These are tabulated in the third column of Table 2. The analysis via single quantum transfer gives somewhat larger values for the rate coefficients for relaxation of $v = 1$ and 2, but approach the values derived from an analysis via Eq. (24) for higher vibrational levels.

The least squares fits to the plots related to the Eq. (30) analysis have near zero intercepts for the lowest vibrational levels, but the intercepts become increasingly larger for the higher vibrational levels. This probably results from neglecting the populations of vibrational levels above 6 in the analysis. As the N_2 vibrational distribution becomes increasingly more quenched, the populations initially in higher levels will cascade down and contribute significantly to the populations of the lower levels. That is, when very little overall quenching has occurred, vibrational levels 7 and above will contribute negligibly to the populations of levels such as 3 or 4. When quenching becomes more significant, however, much of the residual population in levels such as 3 and 4 may well have originated in levels 7 and above. Since the Penning-ionization diagnostic cannot provide information about the populations of these higher levels, our analysis necessarily excludes them from consideration. Were it possible to include them, the ordinates of the points at the larger values of $[\text{SiH}_4]\Delta t$ would undoubtedly be higher. This effect would both increase the slope,

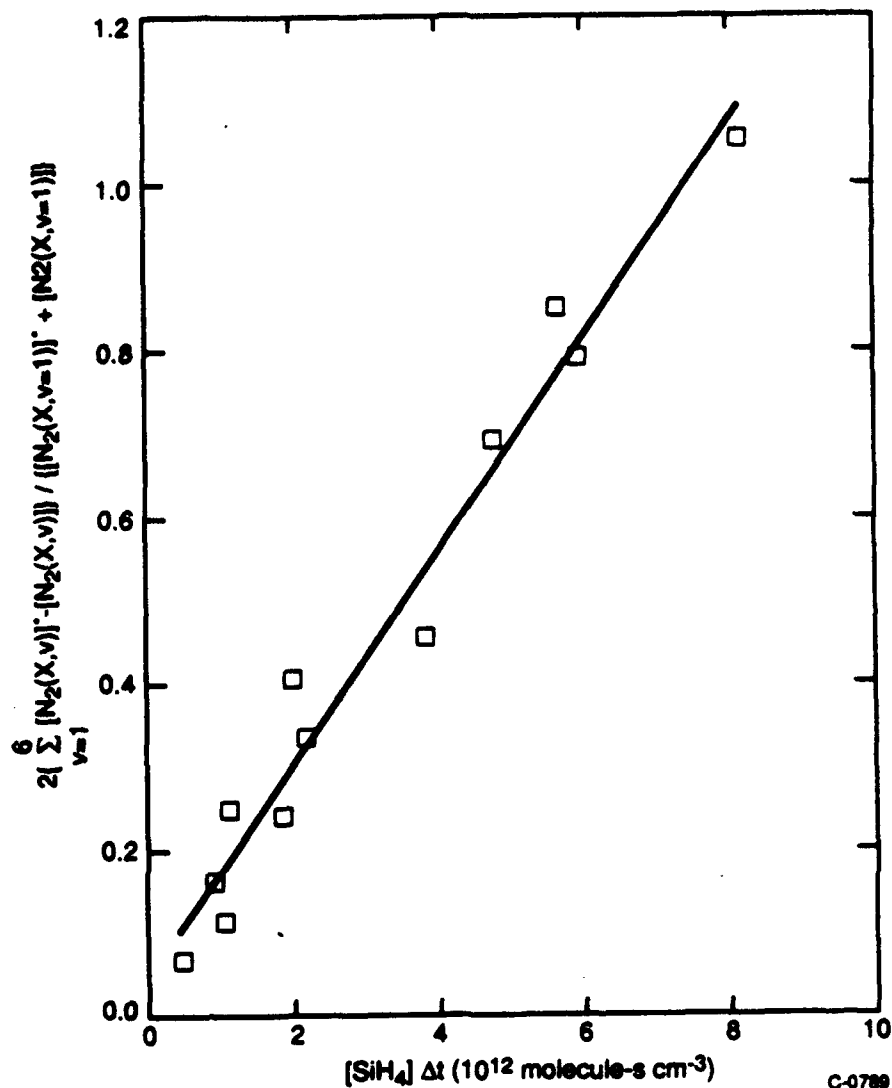


Figure 10. Single quantum analysis of quenching of $N_2(X, v = 1)$ by SiH_4

thus increasing the rate coefficient, and also would lower the intercept, indicating that a sufficiently large set of vibrational levels had been included in the analysis.

The rate coefficient for relaxing vibrational level 1 can also be determined from an analysis of the increase in population of vibrational level 0. In this case the analysis equation is

$$2 \frac{N_0 - N_0^0}{N_1 + N_1^0} = k_{v=1} [SiH_4] \Delta t \quad (31)$$

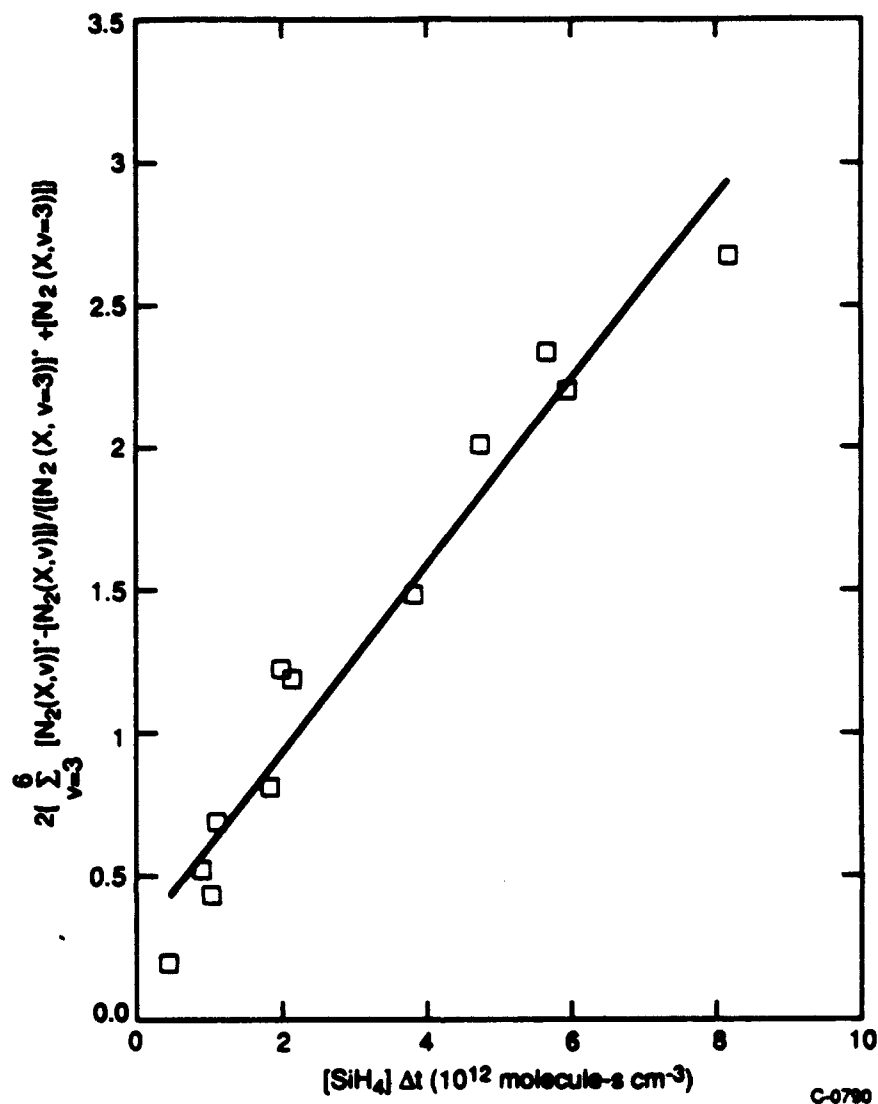


Figure 11. Single quantum transfer analysis of the quenching of $N_2(X, v = 3)$ by SiH_4

This equation results because $v = 0$ has no loss processes, and because in single quantum transfer, only those molecules removed from $v = 1$ can enter $v = 0$. Figure 12 shows the data plot relevant to Eq. (31). The rate coefficient determined from these data is $1.2 \times 10^{-13} \text{ cm}^3 \text{ molecule}^{-1} \text{ s}^{-1}$, in excellent agreement with the value determined by considering the decay of $v = 1$.

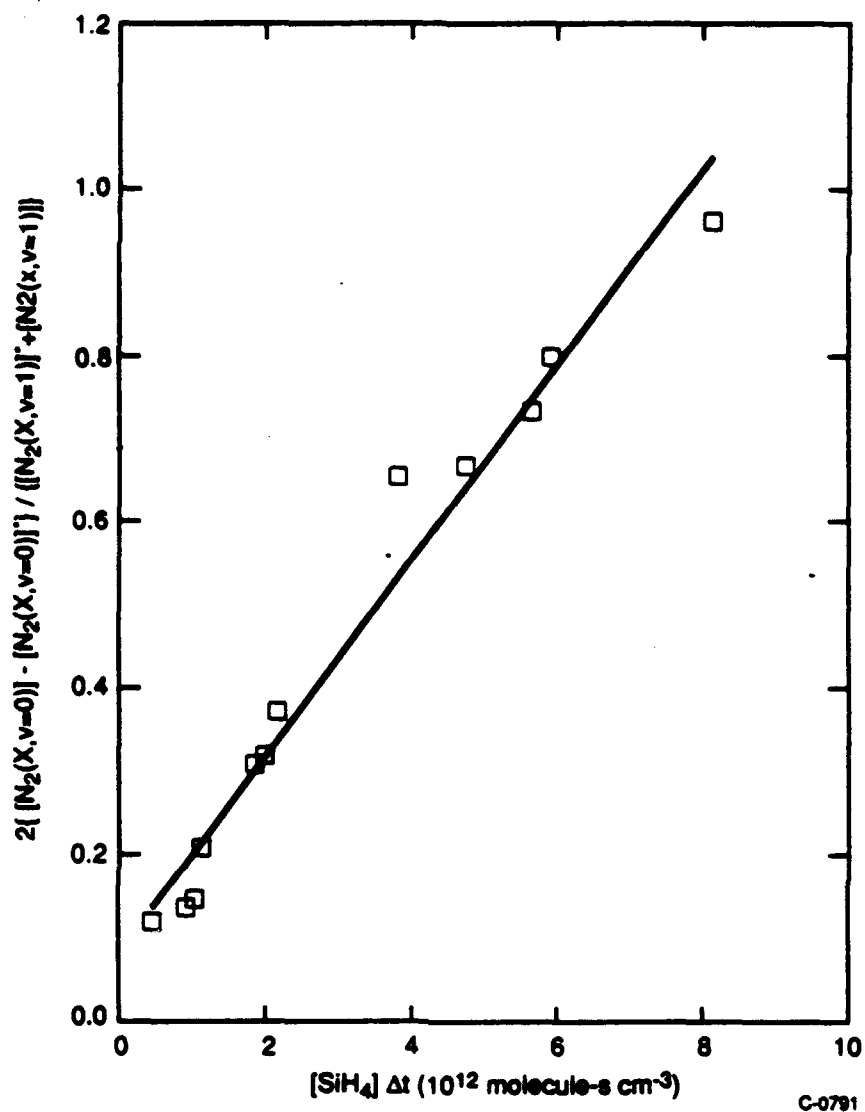


Figure 12. Analysis of the quenching of $N_2(X, v=1)$ by SiH_4 from observations of the increase in $[N_2(X, v=0)]$ as a function of $[SiH_4]$

6. $\text{SiH}_4(\nu_3)$ EXCITATION BY $\text{N}_2(\text{X}, \nu)$

We used the apparatus shown in Figure 2 to investigate the excitation of $\text{SiH}_4(\nu_3)$ by vibration-vibration transfer from $\text{N}_2(\text{X}, \nu)$ to SiH_4 . Because the ν_3 mode of SiH_4 is resonant within kT with single quantum transfer from all $\text{N}_2(\text{X}, \nu \leq 15)$, ν_3 excitation seemed the most logical choice for the efficient quenching reaction. The ν_3 mode fundamental frequency is 2190 cm^{-1} (4570 nm) and its band strength is $625 \text{ cm}^{-2} \text{ atm}^{-1}$ at STP.³⁰ We compared our observations with observations $\text{N}_2\text{O}(\nu_3)$ excitation by $\text{N}_2(\text{X}, \nu)$ when N_2O was added to the reactor. The N_2O ν_3 mode radiates at 2224 cm^{-1} (4500 nm) and its band strength is $1541 \text{ cm}^{-2} \text{ atm}^{-1}$ at STP.³¹

Figure 13 shows the fluorescence spectrum between 4 and 5 μm when SiH_4 is added to a flow of $\text{N}_2(\text{X}, \nu)$. The strong Q-branch of the SiH_4 ν_3 mode is visible at $4.58 \mu\text{m}$ with associated P- and R-branches to either side. The spectral resolution is $0.04 \mu\text{m}$, and the SiH_4 number density is about $1.5 \times 10^{14} \text{ molecules cm}^{-3}$. For comparison, Figure 14 shows the fluorescence spectrum excited when N_2O is added to $\text{N}_2(\text{X}, \nu)$. Here the spectral resolution is $0.01 \mu\text{m}$ and the N_2O number density is about $5 \times 10^{13} \text{ molecules cm}^{-3}$. In addition to the $\text{N}_2\text{O}(\nu_3)$ fundamental band centered at $4.50 \mu\text{m}$, N_2O hot-band emission is evident from $\nu_3=2$ at $4.56 \mu\text{m}$ and $\nu_3=3$ at $4.62 \mu\text{m}$. This demonstrates, that in the case of N_2O quenching at least, multiquantum vibrational energy transfer is efficient.

Figure 15 shows how the emission from $\text{SiH}_4(\nu_3)$ at $4.56 \mu\text{m}$ varies as a function of SiH_4 number density added to the reactor. At low number densities, the emission intensity

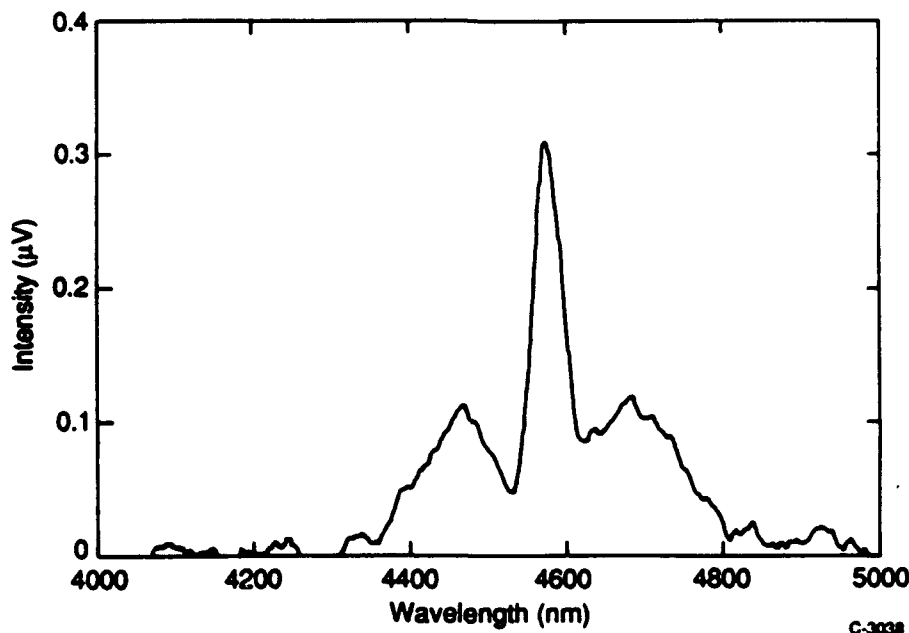


Figure 13. Spectrum of $\text{SiH}_4(\nu_3)$ emission excited by $\text{N}_2(\nu)$

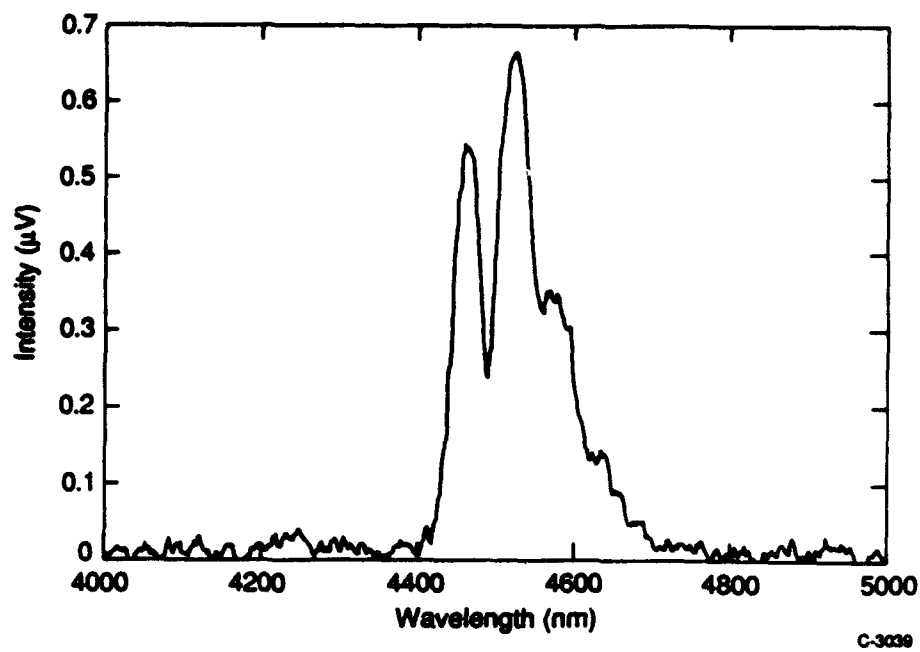


Figure 14. Spectrum of $\text{N}_2\text{O}(\nu_3)$ emission excited by $\text{N}_2(v)$

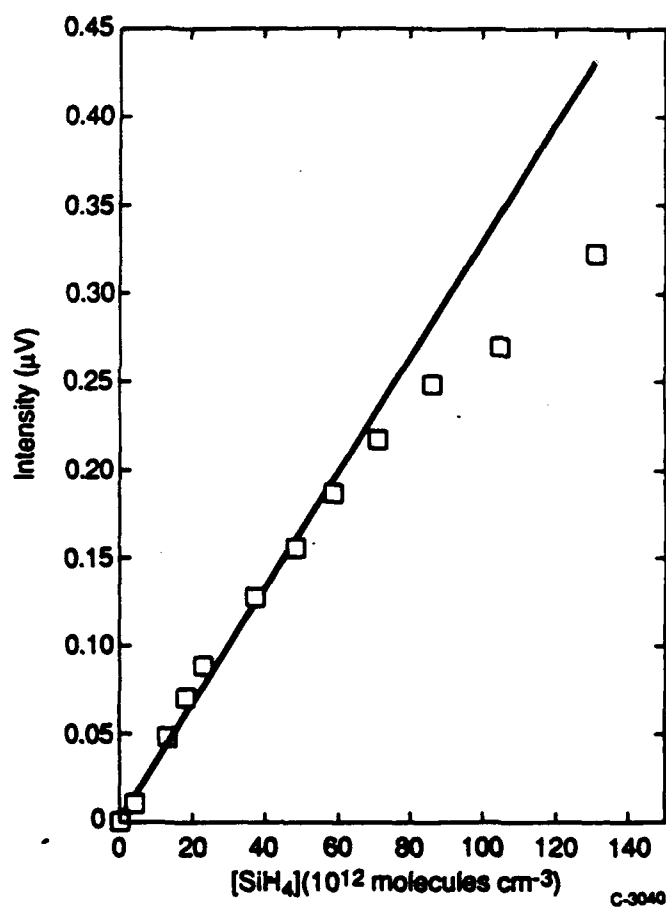
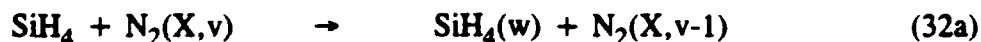


Figure 15. Intensity of $\text{SiH}_4(\nu_3)$ as a function of $[\text{SiH}_4]$ added to $\text{N}_2(X,v)$

increases almost linearly with increases in SiH_4 number density. For higher SiH_4 additions, however, the emission intensity increase is less than linear. Two different effects are responsible for this decrease in linearity. The higher SiH_4 number densities reduce the effective $\text{N}_2(\text{X},\text{v})$ number density in the detector's field of view, thereby lowering the rate of $\text{SiH}_4(\nu_3)$ excitation. In addition, higher number densities of added SiH_4 quench the SiH_4 emission. We can test these suppositions with a simple kinetic model.

We base this model upon the following set of reactions:



Although reaction (35), bath-gas quenching, could not be deduced from the data in Figure 15, the necessity for its inclusion becomes apparent when SiH_4^+ excitation is studied at several different pressures.

With the above reaction scheme, we can write down and solve two differential equations describing the temporal variations in the number densities of $\text{N}_2(\text{X},\text{v})$ and $\text{SiH}_4(\text{w})$. For $\text{N}_2(\text{X},\text{v})$ we have

$$\frac{d[\text{N}_2(\text{X},\text{v})]}{dt} = -k_{32}[\text{SiH}_4][\text{N}_2(\text{X},\text{v})] \quad (36)$$

which can be solved to give

$$[\text{N}_2(\text{X},\text{v})] = [\text{N}_2(\text{X},\text{v})]_0 \exp(-k_{32}[\text{SiH}_4]t) \quad (37)$$

where $[\text{N}_2(\text{X},\text{v})]_0$ is the $\text{N}_2(\text{X},\text{v})$ number density in the absence of SiH_4 . For $\text{SiH}_4(\text{w})$ we have

$$\begin{aligned} \frac{d[\text{SiH}_4(\text{w})]}{dt} = & k_{32a}[\text{SiH}_4][\text{N}_2(\text{X},\text{v})] - (k_{33} + k_{34}[\text{SiH}_4] \\ & + k_{35}[\text{Ar}, \text{N}_2])[\text{SiH}_4(\text{w})] \end{aligned} \quad (38)$$

Using Eq. (37) for $[N_2(X, v)]$, Eq. (38) can be solved to give

$$[SiH_4(w)] = \frac{k_{32a}[N_2(X, v)]_0 [SiH_4] (\exp(-k_{32}[SiH_4]t) - \exp(-(k_{33}+k_{34}[SiH_4] + k_{35}[Ar, N_2])t))}{k_{33}+k_{34}[SiH_4] + k_{35}[Ar, N_2] - k_{32}[SiH_4]} \quad (39)$$

Because we are looking along the axis of the flow reactor, our effective field of view encompasses emissions from volume elements at all axial positions, and thereby reaction times, between zero and the bend in the flow reactor, 36 cm distant from the SiH_4 injector. Thus the observed emission is in reality the integral over time of emission from each of these volume elements. The product of the collection efficiency times the area of each volume element normal to the flow tube axis is constant until the monochromator field of view becomes comparable to the cross-sectional area of the flow tube. This happens in our reactor about 24 cm downstream from the injector. Over the last 12 cm of the field of view, the product of collection efficiency times volume decreases slowly so that at the farthest reaches of the flow reactor, the effective photon emission rates are attenuated by almost a factor of 2 compared to those arising from emission in the first 24 cm of the reactor. Rather than account for this effect exactly, we found it convenient to correct our observations by assuming constant collection efficiency over a column shorter than actually observed. This allows for easier integration of Eq. (39) over time and has a negligible effect on the results provided the effective length of the column is chosen correctly.

The observed emission intensity is then the product of k_{33} times the integrated number density of $SiH_4(w)$ along the length of the observation volume:

$$I = \frac{\zeta k_{32a} k_{33} [N_2(X, v)]_0 [SiH_4]}{k_{33} + k_{34}[SiH_4] + k_{35}[Ar, N_2] - k_{32}[SiH_4]} \times \left\{ \frac{(1 - \exp(-k_{32}[SiH_4]t_0))}{k_{32}[SiH_4]} - \frac{(1 - \exp(-(k_{33} + k_{34}[SiH_4] + k_{35}[Ar, N_2])t_0))}{(k_{33} + k_{34}[SiH_4] + k_{35}[Ar, N_2])} \right\} \quad (40)$$

where t_0 is the effective time along the length of the observation region and the factor ζ is an efficiency factor for the detection system.

We subjected the data in Figure 15 to a least-squares analysis according to Eq. (40) with the unknown parameters being the product $\zeta k_{32a} k_{33} [N_2(X, v)]_0$ and k_{34} . We determined a value for k_{32} from our earlier work to be between 1 and $5.5 \times 10^{-13} \text{ cm}^3 \text{ molecule}^{-1} \text{ s}^{-1}$, depending upon vibrational level, and k_{33} can be calculated from the measured $SiH_4 \nu_3$ band strength. Given a band strength of $625 \text{ cm}^{-2} \text{ atm}^{-1}$, we calculate a radiative decay rate of 28 s^{-1} for the triply degenerate $SiH_4(\nu_3)$. The results of the least-squares fit, for an assumed value $k_{32} = 2.5 \times 10^{-13} \text{ cm}^3 \text{ molecule}^{-1} \text{ s}^{-1}$, are 3.1×10^{-11} for the product $\zeta k_{32a} k_{33} [N_2(X, v)]_0$ and $4.5 \times 10^{-13} \text{ cm}^3 \text{ molecule}^{-1} \text{ s}^{-1}$ for k_{34} . The solid line in Figure 16 compares the results of the fit to the data.

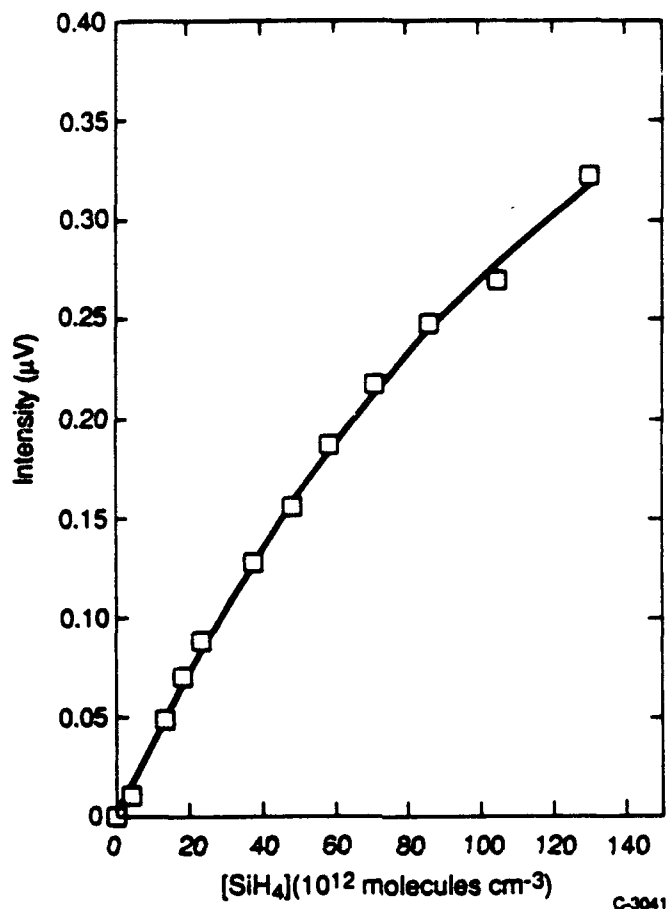


Figure 16. Intensity of $\text{SiH}_4(\nu_3)$ emission as a function of $[\text{SiH}_4]$ added to $\text{N}_2(\text{X}, \nu)$. The solid line is a least-squares fit to Eq. (40) with $k_{32} = 2.5 \times 10^{-13} \text{ cm}^3 \text{ molecule}^{-1} \text{ s}^{-1}$ and $k_{33} = 28 \text{ s}^{-1}$.

To compare with the SiH_4 excitation data, we studied the excitation of $\text{N}_2\text{O}(\nu_3)$ under identical conditions. This affords comparison of the relative excitation efficiencies between the two reactions. A set of equations analogous to Eqs. (32) through (40) also holds for the N_2O data analysis. When necessary we shall prime the k 's for the rate coefficients for the N_2O reactions to distinguish them from those for the SiH_4 reactions.

Data taken at several different pressures are shown in Figure 17 for SiH_4 excitation and Figure 18 for N_2O excitation. It is clear from the way the initial slopes of the SiH_4 data become much smaller for the higher pressure data, in contrast to the near constancy for the N_2O data, that bath gas quenching of $\text{SiH}_4(\nu_3)$ is fairly significant. The variations in the initial slopes can result from the effects of reaction 35 or 35' or from changes in $[\text{N}_2(\text{X}, \nu)]_0$. Because at each pressure the value of $[\text{N}_2(\text{X}, \nu)]_0$ will be the same for both sets of data, we should be able to analyze the data to allow estimation of k_{35} . In addition, by comparing the observed intensities, we should be able to determine a ratio of k_{32a}/k_{32a}' . Values for k_{32} , k_{32}' , and k_{33} , k_{33}' can be estimated from the quenching data and band

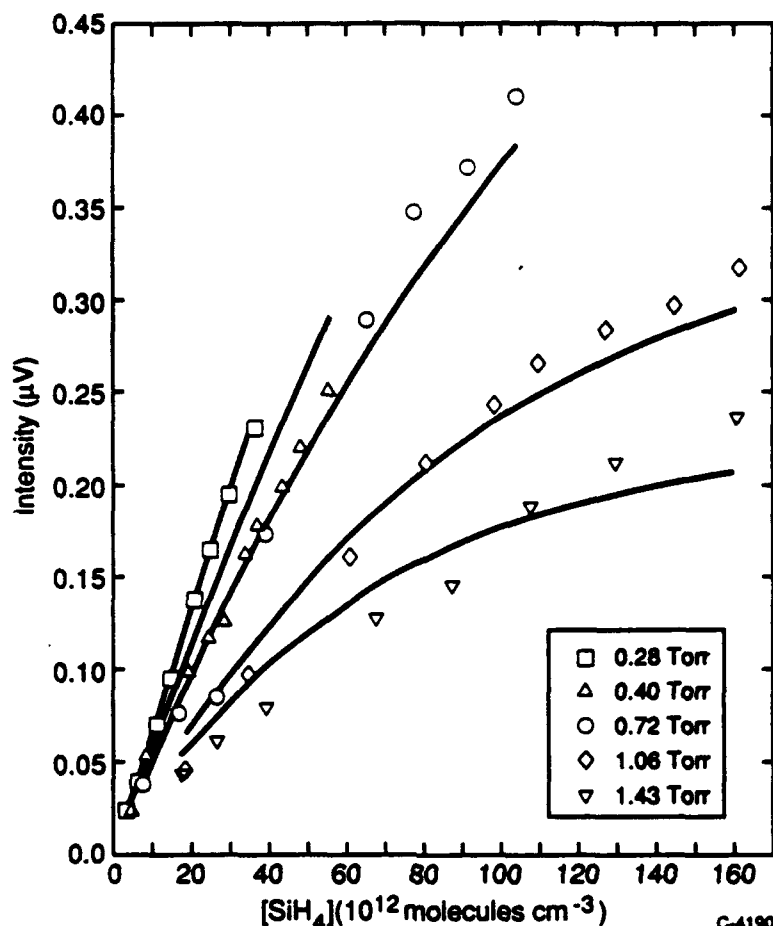


Figure 17. Excitation of $\text{SiH}_4(\nu_3)$ by $\text{N}_2(\text{X}, v)$ at various total argon pressures compared to a kinetic model

strength measurements, respectively. The band strength data give values of k_{33} and k_{33}' of 28 and 214 s^{-1} respectively, while our quenching data indicate a value for k_{32} and k_{32}' of about $2.5 \times 10^{-13} \text{ cm}^3 \text{ molecule}^{-1} \text{ s}^{-1}$ and $1 \times 10^{-13} \text{ cm}^3 \text{ molecule}^{-1} \text{ s}^{-1}$ respectively. For the two parameters we can determine from the data of Figures 17 and 18, the actual values used for k_{32} and k_{32}' aren't particularly important. Variations in both quantities of 30 to 50% give similar results for k_{35} and the ratio k_{32a}/k_{32a}' . The particular values chosen for k_{34} , k_{34}' and k_{35}' can be varied almost at will without affecting the final results for the quantities k_{32a}/k_{32a}' and k_{35} . Our results indicate the ratio k_{32a}/k_{32a}' is 0.35 ± 0.05 and k_{35} is $(6 \pm 2) \times 10^{-15} \text{ cm}^3 \text{ molecule}^{-1} \text{ s}^{-1}$.

Given that the ratio k_{32}/k_{32}' is about 2.5, the result above indicates that $\text{N}_2(\text{X}, v)$ energy transfer to N_2O is about 7 times more efficient at producing infrared radiation at 4500 nm than is energy transfer to SiH_4 . Put another way, if the branching ratio, k_{32a}'/k_{32}' is unity, then only about 15% of the time will an $\text{N}_2(\text{X}, v)$ quantum transferred to SiH_4 appear as radiation at 4500 nm. One reason for this discrepancy is undoubtedly related to the fact that SiH_4 has an infrared inactive vibrational mode, ν_1 , that is also resonant with

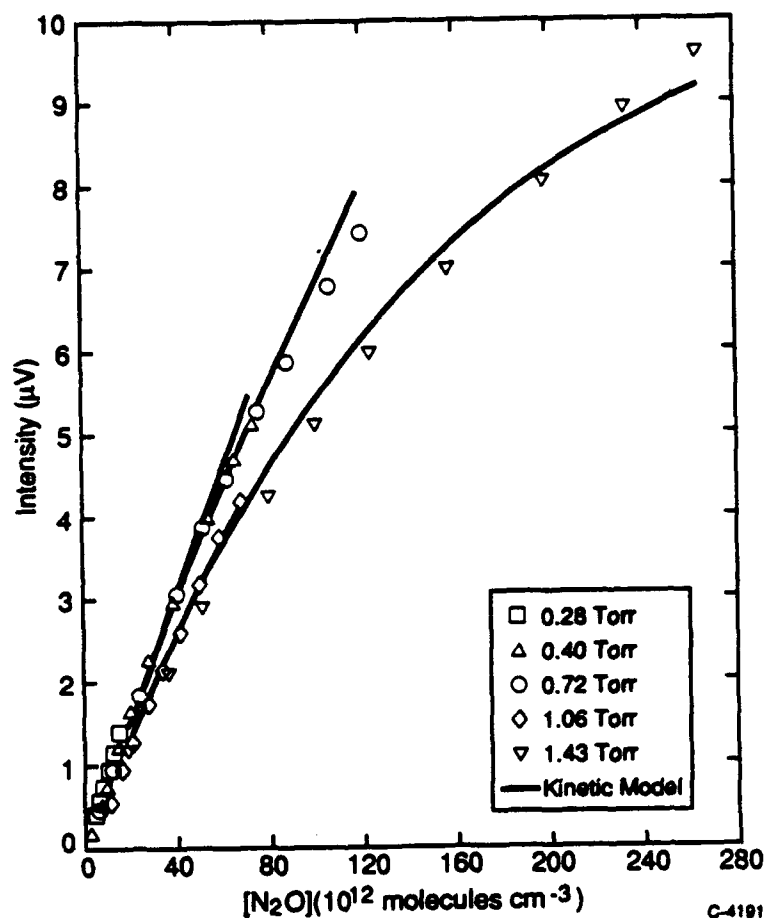


Figure 18. Excitation of $\text{N}_2\text{O}(\nu_3)$ by $\text{N}_2(\text{X}, \nu)$ at various total pressures of argon compared to a kinetic model

$\text{N}_2(\text{X}, \nu)$ one quantum transfer. Evidence for excitation of this band could appear in the infrared in a combination band. Although we searched the region between 2000 and 5000 nm, we saw no other emissions that we could ascribe to SiH_4 infrared radiation. Our system is not particularly sensitive, however, and these bands are likely to be much weaker than the ν_3 band.

7. ALTERNATIVE DETERMINATION OF $N_2(X, v)$ QUENCHING RATE COEFFICIENTS

We measured rate coefficients for $N_2(X, v)$ removal by SiH_4 by monitoring the attenuation in $N_2O(\nu_3)$ radiation when SiH_4 was added to a flow of $N_2(X, v)$ in a 50-cm-long, 2.5-cm-diameter flow tube that was attached at its downstream end to the 5-cm-diameter flow tube used to monitor the infrared radiation. The N_2O was added through the loop injector in the 5-cm-diameter tube directly in front of the CaF_2 window. In this way, N_2O is used as a tracer of $N_2(X, v)$ and changes in $N_2O(\nu_3)$ intensity can be related to changes in $N_2(X, v)$ number density. Unfortunately, because of the need for the long path length to obtain adequate signal levels, the analysis is not completely straightforward. Proper analysis does, however, lead to reasonable results.

Three effects which lead to a reduction in $N_2O(\nu_3)$ intensity when SiH_4 is added at the upstream end of the 2.5-cm-diameter section:

1. quenching of $N_2(X, v)$ in the 2.5-cm section;
2. quenching of $N_2(X, v)$ in the 5-cm section;
3. quenching of N_2O fluorescence by SiH_4 .

The expression for $[N_2O(\nu_3)]$ in the 5-cm-diameter section as a function of distance (time) along the length of the field of view is similar to that given above in Eq. (39). One major difference is that the factor $[N_2(X, v)]_0$ in Eq. (39) becomes $[N_2(X, v)]_0 \exp(-k_{32}[SiH_4]\Delta t_1)$, where Δt_1 is the transit time in the 2.5-cm-diameter tube between the SiH_4 injector and the entrance of the 5-cm-diameter tube. Since our observations are actually proportional to the integrated fluorescence intensity along the length of the 5-cm-diameter section, we have to integrate the product of $k_{33}'[N_2O(\nu_3)]$ over the time the reactants are in the field of view, Δt_2 . The resultant expression is

$$I_{obs} = \frac{k_{32}k_{33}'[N_2O][N_2(X, v)]_0 e^{-k_{32}[SiH_4]\Delta t_1}}{k_{33} + k_{32}[SiH_4] - (k_{32}[N_2O] + k_{32}[SiH_4])} \left\{ \frac{1 - e^{-(k_{32}'[N_2O] + k_{32}[SiH_4])\Delta t_2}}{k_{32}'[N_2O] + k_{32}[SiH_4]} - \frac{1 - e^{-(k_{33} + k_{34}[SiH_4])\Delta t_2}}{k_{33} + k_{34}[SiH_4]} \right\} \quad (41)$$

For the experiments we ran, this expression can be simplified because the product $k_{33}'\Delta t_2$ is sufficiently large that the second exponential term can be neglected. After this simplification and some algebraic manipulation, the expression for the observed intensity becomes

$$I = \frac{k_{32}'[N_2O] [N_2(X, v)]_0 e^{-k_{32}[\text{SiH}_4]\Delta t_1}}{k_{32}'[N_2O] + k_{32}[\text{SiH}_4] \left[1 + \frac{k_{34}'}{k_{33}} [\text{SiH}_4] \right]} \left\{ 1 - \frac{e^{(-k_{32}'[N_2O] + k_{32}[\text{SiH}_4])\Delta t_2}}{1 + \frac{k_{32}[\text{SiH}_4]}{k_{33} \left[1 + \frac{k_{34}'}{k_{33}} [\text{SiH}_4] \right]}} \right\} \quad (42)$$

We fit several sets of decay data to the natural log of Eq. (42), using explicit values for the rate coefficient k_{32}' . Figure 19 compares several sets of data with the best fit curves described by Eq. (42). The results of the fits gave $k_{32} = (2.5 \pm 0.5) \times 10^{-13} \text{ cm}^3 \text{ molecule}^{-1} \text{ s}^{-1}$, and $k_{34}' = (1.1 \pm 0.4) \times 10^{-11} \text{ cm}^3 \text{ molecule}^{-1} \text{ s}^{-1}$. These values were insensitive to 50% variations in k_{32}' . The value for k_{32} derived from this analysis is consistent with values derived by monitoring decays in $N_2(X, v)$. Because the fluorescence of N_2O can be excited by quenching a number of different vibrational levels of nitrogen, we

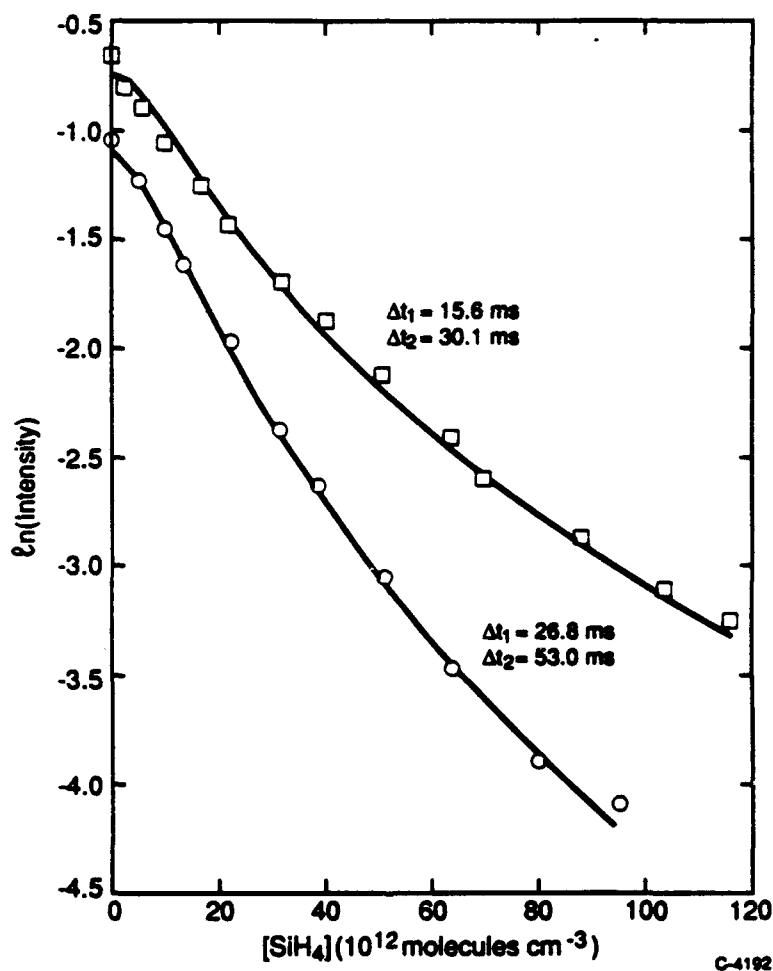


Figure 19. Quenching of $N_2(X, v)$ by SiH_4 using $N_2O(\nu_3)$ fluorescence as a monitor of $[N_2(X, v)]$

would expect this analysis would give a value for k_{32} somewhat larger than that for quenching $v=1$, but smaller than we had observed for quenching $v \geq 5$ or 6. This is exactly what is observed.

8. SILICON NITRIDE COATING EXPERIMENTS

We investigated briefly the coating of sapphire and single-crystal silicon wafers with silicon nitride. We used the technique of infrared absorption spectroscopy to analyze the coatings we produced. In addition to coating the substrates, the experiments generated copious quantities of white powder. Infrared absorption spectra of KBr pellets with small quantities of this powder mixed in showed the powder to be silicon nitride also. Figures 20 and 21 show typical spectra of the film on a silicon substrate and of the powder, respectively. The strong band at around 900 cm^{-1} shows that the samples are silicon nitride. The presence of bands around 3300 cm^{-1} and 1400 to 1050 cm^{-1} indicate the presence of N-H and N-H₂ bonds in the samples, while the small band at 2150 cm^{-1} shows that some SiH bonds are also present.

The structure in the spectrum in Figure 20 between 1800 and 1400 cm^{-1} is not a property of the coating, but rather a peculiarity of the single-crystal silicon wafers used in the coating process. The spectrum was taken with an uncoated wafer in the reference beam of the spectrophotometer. The spectrum of an uncoated wafer between 2000 and 1200 cm^{-1} is also shown in Figure 20. The uncoated wafer also shows structure in the 1800 - 1400 cm^{-1} region. Apparently the small structures in the substrate spectra are amplified when a wafer is used in the reference beam. The referencing procedure is important, however, since silicon has several small absorption bands in the spectral region covered. These bands are removed from the spectral signature of the coating by using an uncoated wafer in the reference beam.

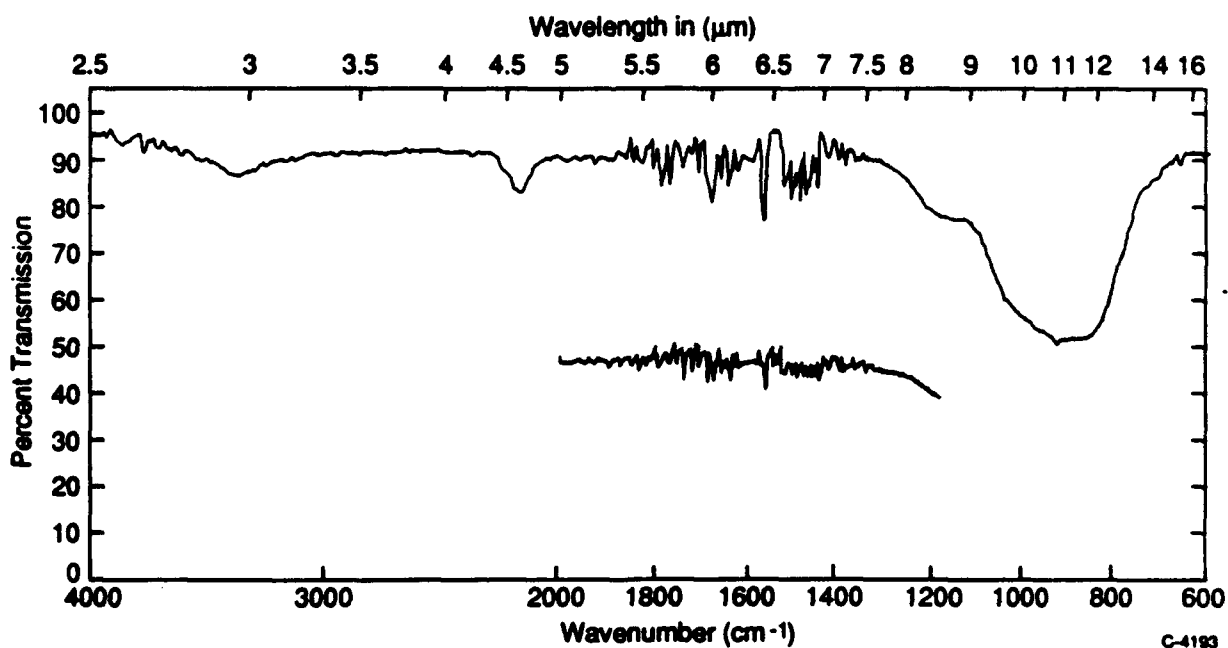


Figure 20. Infrared absorption spectrum of Si₃N₄ on single-crystal silicon

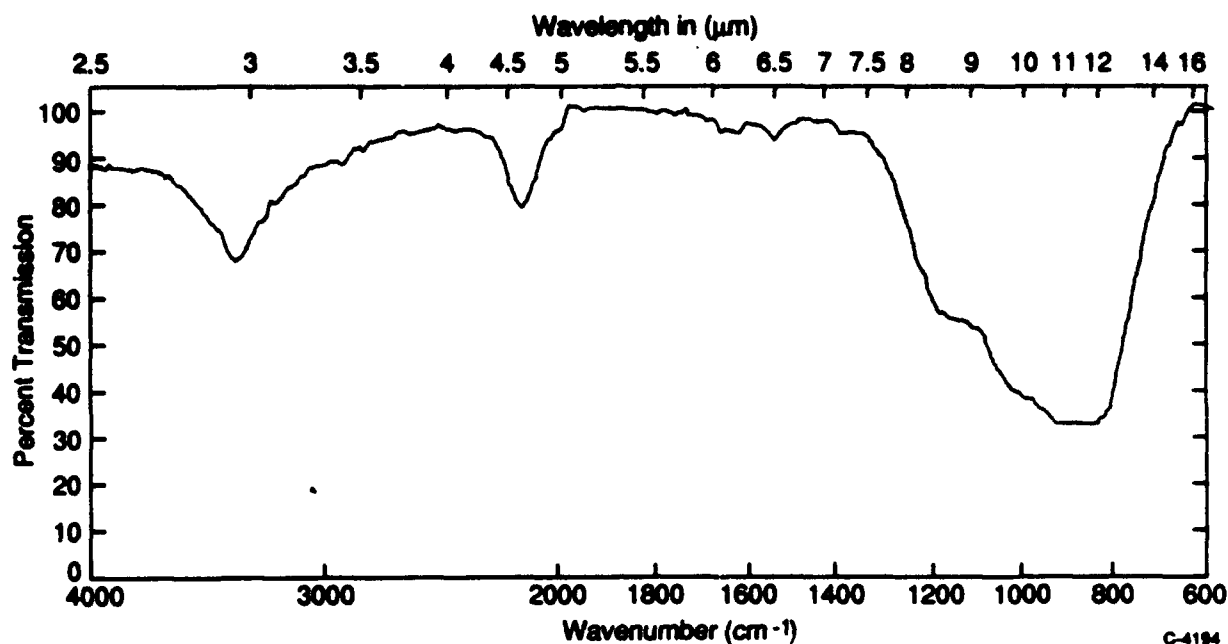


Figure 21. Infrared absorption spectrum of silicon nitride powder in a KBr pellet

Microscopic examination showed the central portions of the coatings to be relatively smooth and uniform. The coating could be scratched rather easily, however. We suspect this results from the incorporation of hydrogen into the coating. We think that reducing the flow rate of silane relative to the active nitrogen would probably lead to reduced hydrogen incorporation. Unfortunately, we were thwarted in our attempts to test this hypothesis.

Our initial apparatus was limited in terms of the minimum SiH_4 flow rates we could achieve. The relatively high SiH_4 flow rates prevented complete decomposition of the silane, which probably explains the presence of so much hydrogen in the films and powder. In order to have smaller flows of SiH_4 , we made a 5% mixture of SiH_4 in argon and stored it in a 5 l bulb on our vacuum line. Several coating experiments with this mixture were disappointing. We apparently developed an air leak in the gas handling system because our coatings with the lower SiH_4 flow rates proved to be silicon oxide rather than silicon nitride.

The silicon nitride powder was generally very fine and had a tendency towards easy agglomeration. It was also very light and was easily dispersed by the merest of air disturbances. In addition, it was strongly affected by small static charges on the surfaces of various laboratory components such as sample jars and microscope slides. Microscopic observation showed that the individual particles were on the order of a micron or less in diameter. In a few instances the powder adhered more tightly to the walls of the flow reactor and was removed essentially as small flakes. The KBr pellet spectrum of the flakes was essentially the same as the fine powder. Qualitatively, it appeared that the quantity of powder formed correlated with the N-atom number densities in the active nitrogen. Although

we did implement a quantitative monitor of N-atom number densities, it was too late in the program to investigate this correlation in a quantitative fashion.

Although our initial kinetic measurements on the quenching of $N_2(X, v)$ by SiH_4 were quite extensive, we saw little evidence that silane was decomposed to a significant extent in these experiments, with one slight exception. The walls of the flow reactor used in the kinetic studies did develop a white film over time just downstream from the $N_2(A)$ injector. Although we didn't analyze this film it is undoubtedly a coating of silicon nitride powder. The reactor walls were still relatively clear upstream from the injector. It would seem, therefore, that the $N_2(X, v)$ itself is not sufficient to decompose the silane sufficiently to form silicon nitride. The presence of the metastables, on the other hand, did allow silicon nitride formation to occur. It is not clear whether the reaction between the metastables and silane dissociated the silane into fragments that could then react with $N_2(X, v)$ to form silicon nitride, or if the silicon nitride formation resulted solely from the interaction of the metastables with the silane and its subsequent decomposition fragments. This is an area that merits further investigation.

9. CONCLUSIONS AND SUGGESTIONS FOR FURTHER STUDY

We showed that silane is extremely efficient at quenching vibrational energy of $N_2(X, v)$. Only about 15% of the energy transferred results in excitation of $SiH_4(\nu_3)$. The rest presumably excites the resonant, but non-infrared active ν_1 mode and other modes outside the spectral bandpass of our detection system.

The success of the single-quantum transfer analysis indicates that single quantum vibration-vibration transfer is the most likely pathway for the energy flow in the system. Our kinetic observations could not rule out, however, the possibility of multiquantum transfer resulting in hot band excitation of SiH_4 or even in direct SiH_4 dissociation. We had hoped to be able to monitor H-atom production in this system, but a number of equipment failures prevented our being able to follow these investigations.

Our limited coating studies showed that adding silane to an active nitrogen afterglow resulted in facile production of both silicon nitride powder as well as in coatings on sapphire and silicon substrates. The quantity of the powder produced seemed to be proportional to the number density of atoms in the afterglow, but we were unable to make these observations quantitative. The lack of significant silicon nitride production in the apparatus used for the kinetic measurements, except in the immediate vicinity of the metastable injector, shows that vibrationally excited nitrogen by itself does not appear to be sufficient for silicon nitride formation. Whether or not it enhances silicon nitride production in the presence of atoms or metastables is still not clear. Since the reaction of atomic nitrogen with silane is endoergic, it seems likely that $N_2(X, v)$ is necessary to promote efficient silicon nitride synthesis. This may not be the case; however, it could be adequate just to have N atoms and electronically excited molecular metastables present. The primary product of N-atom recombination is $N_2(B^3\Pi_g)$, and our kinetic studies show that silane quenches this species with extraordinary efficiency.

Future investigations should focus more directly on the coating process itself. Using techniques we have developed and implemented in this program, measuring coating efficiencies under conditions where the N-atom and $N_2(X, v)$ number densities are carefully monitored and controlled should be straightforward. If $N_2(X, v)$ appears not to be particularly important in the silicon nitride formation processes, then the relative importance of electronically excited nitrogen molecules in the silane decomposition processes should be investigated. This can be done in two ways. Varying the reactor pressure under conditions of constant N-atom number density allows the production rates of electronically excited nitrogen to be varied in a controlled fashion. In addition, one could make metastables in the absence of atomic nitrogen and monitor changes in silicon nitride formation when these metastables are added to a flow of N atoms.

10. REFERENCES

1. G. Lucovsky, and D.V. Tsu, "Plasma enhanced chemical vapor deposition: Differences between direct and remote plasma excitation," *J. Vac. Sci. Technol.* A5, 2231 (1987).
2. D.V. Tsu and G. Lucovsky, "Silicon nitride and silicon dimide grown by remote plasma enhanced chemical vapor deposition," *J. Vac. Sci. Technol.* A4, 460 (1986).
3. G. Lucovsky, P.D. Richard, D.V. Tsu, S.Y. Lin, and R.J. Markunas, "Deposition of silicon dioxide and silicon nitride by remote plasma enhanced chemical vapor deposition," *J. Vac. Sci. Technol.* A4, 681 (1986).
4. J.L. Jauberteau, D. Conte, M.I. Baraton, P. Quinard, J. Aubreton, and A. Catherinot, "Deposition of Silicon Nitride thin films by reaction of SiH_4 in a nitrogen post-discharge," *Plasma Chem. Plasma Proc.* 10, 401 (1990).
5. L. Bardos, J. Musil, and P. Taras, "Differences between microwave and RF activation of nitrogen for the PECVD process," *J. Phys. D: Appl. Phys.* 15, L79 (1982).
6. C.A. DeJoseph, "Reactions of Silane in active nitrogen," WRDC-TR-90-2001, Final Report (1990).
7. Thermochemistry is from the following references:
 - a. J. Berkowitz, J.P. Greene, and H. Cho, "Photoionization mass spectrometric studies of SiH_n ($n=1-4$)," *J. Chem. Phys.* 86, 1235 (1990).
 - b. S.T. Gibson, J.P. Greene, and J. Berkowitz, "Photoionization of the amidogen radical," *J. Chem. Phys.* 83, 4319 (1985).
 - c. JANAF Thermochemical Tables, Natl. Stand. Ref. Data Ser., *Natl. Bur. Stand.* 37 (1971) and succeeding supplements.
 - d. L.G. Piper, "On the heat of formation of NH ," *J. Chem. Phys.* 70, 3417 (1979).
8. L.G. Piper and G.E. Caledonia, "Kinetics of Silane Decomposition by Atomic and Molecular Nitrogen Metastables," *J. Phys. Chem.* 95, 698 (1991).
9. O. Horie, P. Potzinger and B. Reimann, "Chemiiionization and chemiluminescence in the reaction of SiH_4 with active nitrogen," *Chem. Phys. Lett.* 129, 231 (1986).
10. J.F. O'Keefe and F.W. Lampe, "Spectroscopic detection of silylene in the infared multiphoton decomposition of silane," *Appl. Phys. Lett.* 42, 217 (1983).

11. L.G. Piper, "The Excitation of $N_2(B^3\Pi_g, v=1-12)$ in the Reaction Between $N_2(A^3\Sigma_u^+)$ and $N_2(X, v \geq 5)$," *J. Chem. Phys.* **91**, 864 (1989).
12. L.G. Piper, K. Donohue, W.J. Kessler, T.R. Tucker, W.P. Cummings, W.J. Marinelli, and S.J. Davis, "Laser-Based Diagnostics for $N_2(X, v)$," PSI-TR-960, Final Report to the Air Force Weapons Laboratory under Contract No. F29601-87-C-0056 (1990). Also published by the Weapons Laboratory (AFSC) as WL-TR-90-45. Available from NTIS.
13. L.G. Piper, "Further Observations on the Excitation of $IF(B^3\Pi_0^+)$ in Active Nitrogen," *J. Phys. Chem.* **95**, 3965 (1991).
14. D.H. Stedman and D.W. Setser, "Chemical Application of Metastable Argon Atoms II. A Clean System for the Formation of $N_2(A^3\Sigma_u^+)$," *Chem. Phys. Lett.* **2**, 542 (1968).
15. L.G. Piper, L. Gundel, J.E. Velazco, and D.W. Setser, "Excitation of Nitrogen and Carbon Monoxide Ionic Emissions by $He(2^3S)$, He^+ and He_2^+ ," *J. Chem. Phys.* **62**, 3883 (1975).
16. L.G. Piper, K.W. Holtzclaw, B.D. Green, and W.A.M. Blumberg, "Experimental Determination of the Einstein Coefficients for the $N_2(B-A)$ Transition," *J. Chem. Phys.* **90**, 5337 (1989).
17. L.G. Piper and W.J. Marinelli, "Determination of Non-Boltzmann Vibrational Distributions of $N_2(X, v)$ in He/N_2 Microwave-Discharge Afterglows," *J. Chem. Phys.* **89**, 2918 (1988).
18. L.G. Piper and W.P. Cummings, "Characterization of $N_2(X, v)$ in the Effluents of Common Laboratory Discharges Using $He^*(2^3S)$ Penning Ionization," PSI-SR-445, manuscript in preparation (1990).
19. L.G. Piper, "Energy Transfer Studies on $N_2(X^1\Sigma_g^+, v)$ and $N_2(B^3\Pi_g)$," *J. Chem. Phys.* **97**, 270 (1992).
20. L.G. Piper, "Further Observations on the Nitrogen Orange Afterglow," *J. Chem. Phys.* **99**, xxxx (1993).
21. A.L. Schmeltekopf, E.E. Ferguson, and F.C. Fehsenfeld, "Afterglow Studies of the Reaction of He^+ , $He(2^3S)$, and He_2^+ with Vibrationally-Excited N_2 ," *J. Chem. Phys.* **48**, 966 (1968).
22. S.J. Young, and K.P. Horn, "Measurement of Temperatures of Vibrationally Excited N_2 ," *J. Chem. Phys.* **57**, 4835 (1972).

23. S.J. Young, "Measurement of Vibrational Temperature of CO and N₂ Using the He(2³S) Penning Ionization Technique," *J. Chem. Phys.* **38**, 1603 (1973).
24. L.G. Piper, S.J. Davis, H.C. Murphy, W.C. Cummings, L.P. Walkauskas, M.A. DeFaccio, L.M. Cowler, W.T. Rawlins, W.J. Marinelli, and B.D. Green, "CONAN: Chemistry of Nitrogen-A Nascence," Final Technical Report PSI-076/TR-593 for the period 4 September 1984 through 4 June 1986 under Contract No. F29601-84-C-0076, January 1987. Also published by the Weapons Laboratory (AFSC) as AFWL-TR-86-95. Available from NTIS.
25. C.E. Treanor, J.W. Rich, and R.G. Rehm, "Vibrational Relaxation of Anharmonic Oscillators with Exchange Dominated Collisions," *J. Chem. Phys.* **43**, 1798 (1968).
26. G.E. Caledonia, and R.E. Center, "Vibrational Distribution Functions in Anharmonic Oscillators," *J. Chem. Phys.* **55**, 552 (1971).
27. M. Dilonardo, and M. Capitelli, "Non-Equilibrium Dissociation of Nitrogen," *Rev. Phys. Appl.* **13**, 115 (1978).
28. S.J. Davis, and L.G. Piper, "The Production of N₂(B³Π_g, v=1-12) in the Reaction Between NF(a¹Δ) and N(²D)," *J. Chem. Phys.* **94**, 4515 (1990).
29. O. Stern, and M. Volmer, "Über die Abklingungszeit der Fluoreszenz," *Physik. Zeitschr.* **20**, 183 (1919).
30. W.D. Allen and H.F. Schaefer III, "Geometrical Structures, Force Constants and Vibrational Spectra of SiH₂, SiH₃, and SiH₄," *Chem. Phys.* **108**, 243 (1986).
31. R.H. Kagan, "Infrared Absorption Intensities of N₂O," *J. Mol. Spectrosc.* **95**, 297 (1982).